REPORT DOCUMENTATION PAGE

Form Approved
OMB No. 0704-0188

AD-A278 941

2. REPORT DATE	3. REPORT TYPE AND DATES COVERED
1994 April 7	Annual 2/1/93-1/31/94

(U) Detailed Studies of Soot Formation in Laminar Diffusion Flames for Application to Modeling Studies

5. FUNDING NUMBERS

PE - 61102F
PR - 2308
SA - BS
G - F49620-92-J-0161

6. AUTHOR(S)

Robert J. Santoro

7. PERFORMING ORGANIZATION NAME(S) AND ADDRESS(ES)

The Pennsylvania State University
Department of Mechanical Engineering
University Park, PA 16802

8. PERFORMING ORGANIZATION REPORT NUMBER

AFOSR-TR- 94 0264

9. SPONSORING/MONITORING AGENCY NAME(S) AND ADDRESS(ES)

AFOSR NA
110 DUNCAN AVE SUITE B115
BOLLING AFB DC 20332-0001

10. SPONSORING/MONITORING AGENCY REPORT NUMBER

11. SUPPLEMENTARY NOTES

12a. DISTRIBUTION/AVAILABILITY STATEMENT

Approved for public release; distribution is unlimited

12b. DISTRIBUTION CODE

13. ABSTRACT (Maximum 200 words)

An investigation of soot formation in laminar diffusion flames has shown that soot particle surface growth under laminar diffusion flame conditions ceases because of the depletion of hydrocarbon species, in particular acetylene and benzene, and not due soot particle reactivity loss due to thermal aging of the particles. This results has been obtained through direct species concentration measurements under well controlled conditions while the particle reactivity effects were calculated based on premixed flame results along with particle temperature/time information available from earlier laminar diffusion flame studies. Comparisons with a soot formation model which incorporated detailed chemistry effects showed good agreement in terms of predicted and measured species concentration and soot particle field evolution. In addition, a novel technique for measuring soot volume fraction has been developed based on laser-induced incandescence and applied to similar laminar diffusion flame studies with good success. This technique represents a major development in terms of its ability to make soot volume fraction measurements in unsteady inhomogeneous combusting flows.

14. SUBJECT TERMS

Soot Formation, Soot Particles, Diffusion Flames

15. NUMBER OF PAGES

95

16. PRICE CODE

17. SECURITY CLASSIFICATION OF REPORT	18. SECURITY CLASSIFICATION OF THIS PAGE	19. SECURITY CLASSIFICATION OF ABSTRACT	20. LIMITATION OF ABSTRACT
Unclassified	Unclassified	Unclassified	UL

NSN 7540-01-280-5500

Standard Form 298 (890104 Draft)
Prescribed by ANSI Std. 239-18
298-01

Annual Report

on

Detailed Studies of Soot Formation in Laminar Diffusion Flames

for Application to Modeling Studies

AFOSR Grant F49620-92-J-0161

Prepared by

Robert J. Santoro
Department of Mechanical Engineering
The Pennsylvania State University
University Park, PA 16802

Submitted to

Air Force Office of Scientific Research
Bolling Air Force Base
Washington, DC

April 1994

Table of Contents

Summary

An investigation of soot formation in laminar diffusion flames has shown that soot particle surface growth under laminar diffusion flame conditions ceases because of the depletion of hydrocarbon species, in particular acetylene and benzene, and not due soot particle reactivity loss due to thermal aging of the particles. This results has been obtained through direct species concentration measurements under well controlled conditions while the particle reactivity effects were calculated based on premixed flame results along with particle temperature/time information available from earlier laminar diffusion flame studies. Comparisons with a soot formation model which incorporated detailed chemistry effects showed good agreement in terms of predicted and measured species concentration and soot particle field evolution. In addition, a novel technique for measuring soot volume fraction has been developed based on laser-induced incandescence and applied to similar laminar diffusion flame studies with good success. This technique represents a major development in terms of its ability to make soot volume fraction measurements in unsteady inhomogeneous combusting flows.

1.0 Research Objectives

The objective of this research effort is to investigate the fundamental phenomena controlling soot particle formation and destruction in combustion systems. The emphasis and approach chosen for the present studies is based on previous results developed under AFOSR support which have proven the soundness of the methodology being utilized [1-10]. The present studies are conducted in a series of well-characterized laminar diffusion flames in which fuel constituents, temperature, concentration and transport processes are systematically varied and/or measured. A laminar diffusion flame environment has been selected because it provides a relatively simple environment in which mixing processes are important while allowing for a wide range of measurement techniques to be employed. The importance of mixing in practical combustor situations is well recognized and, thus, it is critical to study soot formation processes under conditions where mixing has a significant role.

Specifically, the current effort emphasizes detailed measurements of the preparticle chemistry, particle inception and surface growth phenomena important in soot particle formation. These studies are intended to yield quantitative measurements of the precursor and surface growth species which contribute to soot particle formation and growth. Data, which is temporally and spatially resolved, are of great value to modeling studies as past studies have demonstrated [11-14]. In fact, the availability of such results has allowed significant progress to be achieved over the past decade in soot modeling capabilities. In particular, current modeling studies being conducted by Prof. M. Frenklach at Penn State will be very beneficial in terms of providing comparisons with the present measurements.

During the second year of this study, efforts have continued to emphasize measurements of species concentration, especially acetylene and benzene concentrations, throughout the flame using both mass spectrometry and gas chromatography. Analysis has concentrated on explaining the soot surface growth process with respect to particle aging, and to collaborating in a soot modeling effort with Prof. Ian Kennedy of the University of California. Additionally, a new approach for obtaining quantitative soot volume fraction measurements using laser-induced incandescence has been developed and demonstrated. In the following sections, the techniques used and results obtained during this past year will be summarized. More detailed discussions are included in the appendices for most of the results. For this reason, the main body of the report will strive for concise presentations of the results.

2.0 Research Approach

For the present studies, a coannular laminar diffusion flame has been selected for study. This flame configuration has been widely studied recently and has been the focus of extensive fuel

molecular structure and pressure sensitivity studies in our laboratory [1-10]. Since practical combustors typically involve the separate injection of fuel and oxidizer, laminar diffusion flames provide a simple, tractable environment in which to study soot formation while maintaining conditions where mixing effects are important. Soot formation can be viewed as a series of sequential processes which occur to some degree in all combustion environments where soot is observed. It is the relative importance of these processes and their coupling which determines the amount of soot formed, its distribution throughout the combustion zone and its eventual emission from a specific combustor. Essential to the study of these processes is the selection of an experimental configuration which can provide the range of conditions typical of fuel-rich combustion zones. Laminar coannular diffusion flame studies have clearly demonstrated that such conditions can be achieved and studied [5]. Furthermore, such studies are proving to be increasingly valuable for the validation of modeling studies. With these points in mind, the coannular laminar diffusion flame represents a highly attractive experimental configuration for the present studies.

The studies during the current year have been conducted in an atmospheric diffusion flame facility consisting of a coannular diffusion flame burner, burner chimney, positioning system and gas metering system. The burner has a configuration consisting of a 1.1 cm fuel tube surrounded by a 10 cm air annulus. The air passage is partially filled with glass beads followed by a series of fine screens to provide flow conditioning. A ceramic honeycomb 2.54 cm in thickness is used at the exit to provide a uniform flow field. The fuel tube which extends 4.8 mm above the ceramic honeycomb also is partly filled with glass beads to condition the flow. The fuel flow can consist of up to three gases, each metered with a separate rotameter. This allows for mixtures of fuels as well as nitrogen dilution of the fuel for temperature and concentration variation. The air flow is metered using a mass flowmeter or rotameter which can monitor flows up to 5 SCFM of air. To protect the flame from room disturbances, a metal chimney has been incorporated into the burner facility. The chimney translates horizontally with the burner while the burner slides vertically within the chimney. Slots machined in the chimney provide access for the optical and intrusive probing of the flame.

A variety of diagnostic techniques are available for application to these studies to measure the soot particle, temperature, species concentration and velocity fields. Both non-intrusive laser-based techniques, such as laser light scattering, laser velocimetry, laser-induced incandescence and laser-induced fluorescence, and intrusive probing followed by mass spectrometric and gas chromatographic analysis are utilized in these studies. A brief description of the apparatus used for these measurements follows for the reader's information.

2.1 Pulse Laser Systems

An Nd-YAG pulsed-dye laser system is utilized for fluorescence detection of OH radicals as well as for PAH species measurements while the Nd-YAG laser alone provides the light source for the laser-induced incandescence measurement. The major components of the system involve the dye laser, which consists of an Nd-YAG pulsed laser operating at 532 nm, a dye laser module and a doubling crystal. The present system has the capability to tune over a wavelength range extending from 220 to 600 nm. This wavelength range is quite suitable for OH fluorescence as well as PAH measurements. Detection is achieved using a photomultiplier or an intensified CCD array camera. In the case of the photomultiplier (PMT), the PMT signal is input to a box car integrator to provide for signal averaging and background noise rejection. For the intensified CCD array camera, direct storage of the images on a personal computer is used to record the data. This unit has a 50 ns gate capability and can be used for signal averaging of multiple laser shots. Using this camera, planar laser imaging is also possible, which allows spatially extensive measurements to be obtained.

2.2 Intrusive Probe Sampling for Species Concentration Measurements

In order to provide more quantitative information on the species important in the formation and growth of soot particles, a mass spectrometer system has been assembled for these studies. Gas samples from the flames under study are obtained using a quartz microprobe technique similar to the approach taken by Smyth *et al.* [15]. Measurements of gas phase species in the soot precursor and particle inception regions can be obtained. Measurements in the present studies are also extended into the surface growth region in order to ascertain the important species responsible for mass addition through surface growth. As part of the current research program, approaches allowing sampling of fuel-rich particle laden regions have been developed which allow measurements in the post-particle inception region of the flame. Sampling probe techniques usually are limited by orifice clogging problems which can only be overcome by increasing the orifice dimensions and sacrificing the spatial resolution of the measurements. To overcome the aforementioned orifice clogging problem, a novel sonic sampling probe has been developed and applied to a series of laminar diffusion flames containing various amounts of soot. The details of the design and operation of this probe were previously presented [16].

The approach, employed to prevent clogging of the probe orifice, involves mechanically oscillating a wire through the orifice region using a spring-loaded solenoid plunger whose driving circuit is electronically interrupted periodically (see Figures 1 and 2). The constant motion of the wire relative to the quartz tube is responsible for keeping the orifice open. For the present probe, the effective orifice is the annulus formed by an oscillating 130 μm diameter Sapphire fiber of uniform

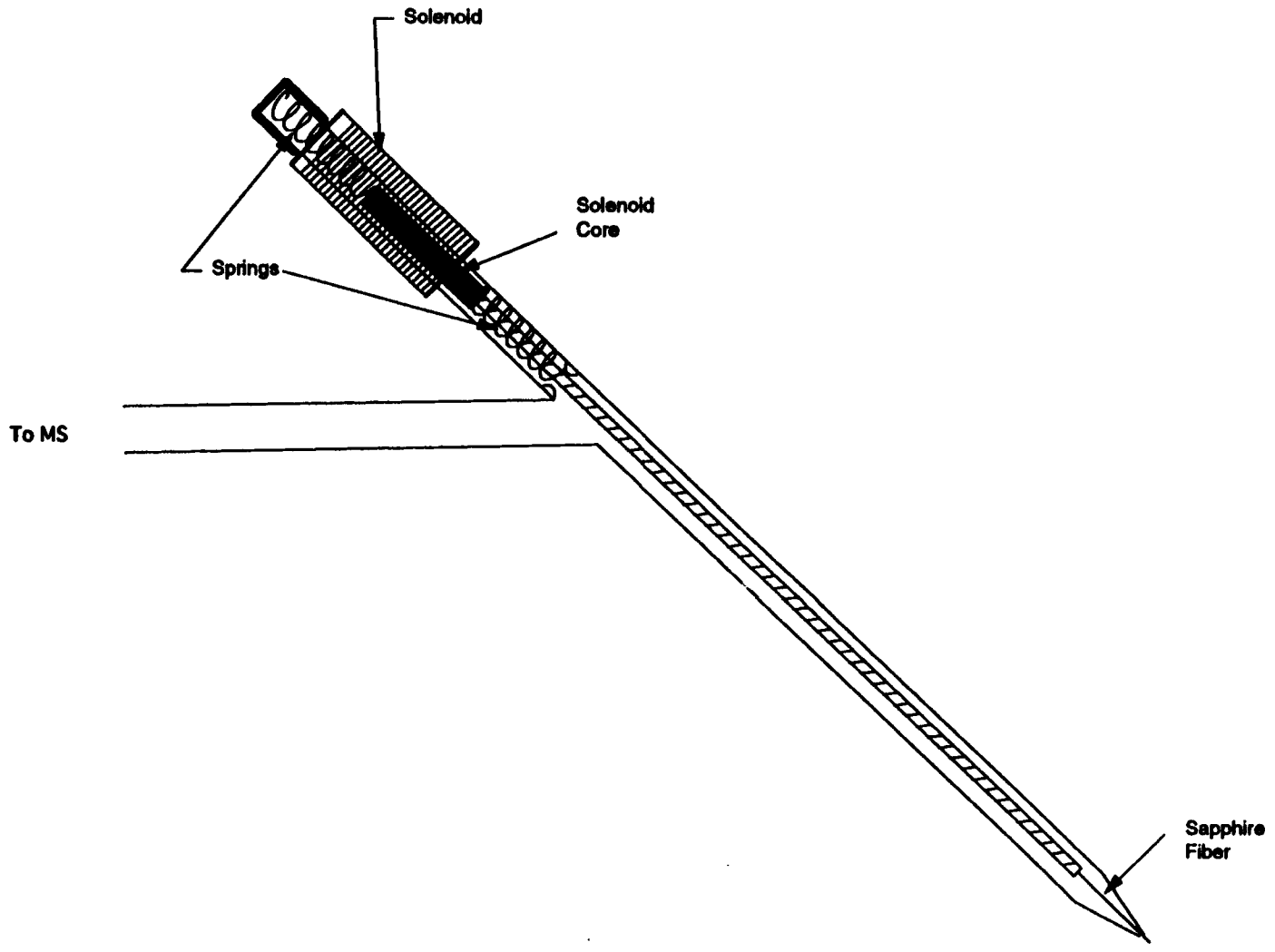

Figure 1. Schematic representation of the electromagnetic sonic probe.

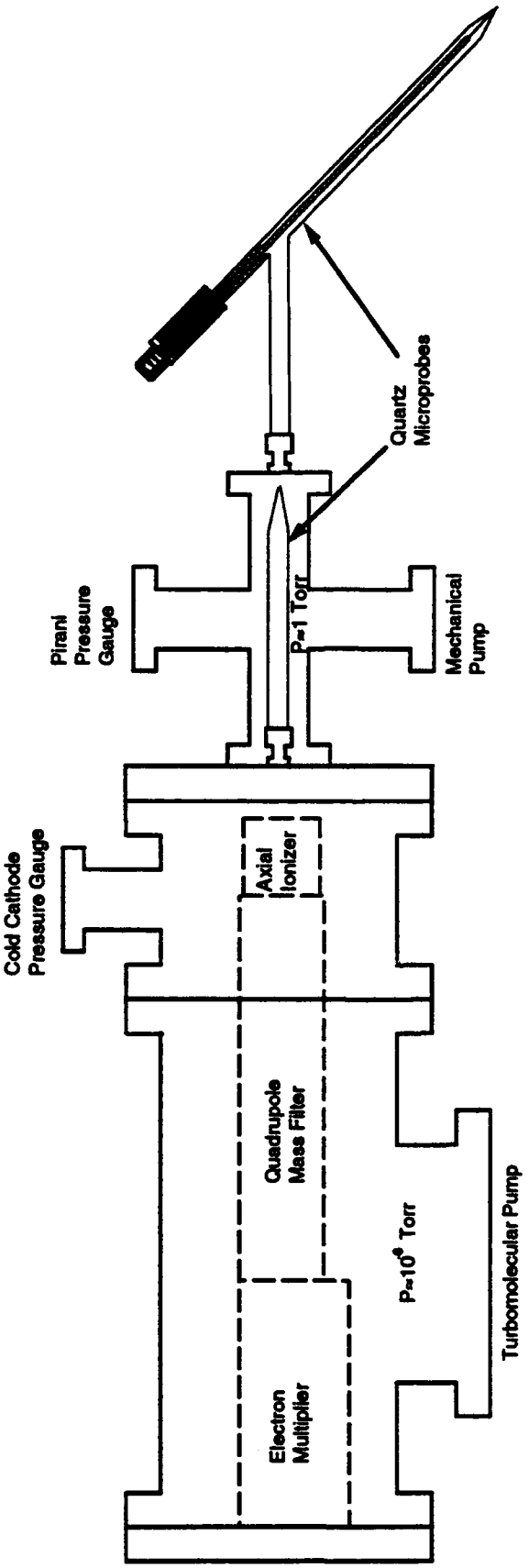

Figure 2. Schematic representation of the quadrapole mass spectrometer and probe assembly.

cross section and the 160 μm diameter orifice in the quartz tube. Therefore, the effective orifice is equivalent to approximately a 100 μm circular hole. The Sapphire fiber is attached to a 1.59 mm tube which is connected to a spring-loaded soft iron solenoid plunger which oscillates in the orifice. This probe is referred to as the electromechanical sonic probe (EMS) since it employs a sonic sampling orifice with an electromagnetic mechanism to maintain the integrity of the orifice opening.

The mass spectrometer used for these studies utilizes a quadrupole mass filter with a mass range of 1 to 500 amu. This unit (an Extrel Model C-50) has excellent mass resolution (0.1 amu) and high sensitivity. A gas chromatograph (Hewlett-Packard 5860) is also used for gas analysis to complement the mass spectrometer measurements. This system utilizes a specially designed sampling and pressurization approach to allow the EMS probe to be used (see appendix A). Radial profiles of the species concentration as a function of axial position are obtained by traversing the flame in the radial direction. When these measurements are combined with the soot particle and velocity measurements, the temporal evolution of the species concentration and its relationship to soot formation can be investigated.

3.0 Research Accomplishments

In the following sections the research accomplishments which have been achieved during the current year of the grant are summarized. Specifically, three areas of activities are described: (1) soot particle surface growth mechanisms, (2) soot modeling studies and (3) laser-induced incandescence measurements of soot volume fraction.

3.1 Soot Particle Surface Growth Mechanisms

Extensive spatially resolved measurements of the species concentration field have been obtained with both mass spectrometry and gas chromatography analysis approaches for a well-studied ethene/air laminar diffusion flame. The complete set of mass spectrometry measurements obtained previously has been repeated to allow for an estimation of the accuracy and precision of the measured data. This information is critical for modeling comparisons in order to accurately assess when real differences exist between measurement and prediction. Additionally, similar spatially resolved concentration measurements were obtained with a gas chromatography approach to provide an independent measurement of the concentrations for comparison with the mass spectrometer data. The gas chromatograph also allowed determinations of the concentrations of some key species not easily measured with the mass spectrometer, in particular carbon monoxide.

The major conclusions of these studies were:

1. Soot particle surface growth terminates because of the depletion of the hydrocarbon species

responsible for surface reactions which add mass to the particle. In particular, the measurements of acetylene and benzene clearly show these species decrease to trace concentration levels at the peak of the soot volume fraction location.

2. Comparisons with results describing the aging process, which soot particles have been observed to experience under premixed flame conditions, show that this mechanism has only a small contribution to the reduction in the surface growth rate for these laminar flame conditions.

These conclusions are consistent with recent work by Honnery and Kent [17,18], who have shown that in long laminar diffusion flames, soot growth can be extended to very long residence times. A more detailed discussion of these results is contained in Appendix A where the data and analysis to support the above conclusions are presented.

3.2 Soot Modeling Studies

A collaborative effort was initiated with Prof. Ian Kennedy of the University of California at Davis to compare the measured soot and species concentrations fields with that predicted by a model developed by Prof. Kennedy and his co-workers. A system of elementary reactions were used to describe the gas phase C_1 and C_2 chemistry. The model incorporates a simple description of the growth of soot particles which performs a good job of reproducing the amount of soot in the flame and the transition from non-sooting to sooting conditions. Stable gas phase species measured in the flame along with OH concentrations previously obtained [10] were compared with model predictions. The model reproduced most of the specified concentration profiles quite well. It was found that the assumption of equilibrium concentrations for the minor radical species was grossly in error, particularly near the end of the flame where temperatures were low. Calculated radical species were found in concentrations that were orders of magnitude greater than equilibrium. Comparisons with measured OH concentrations supported this observation. The results of this work represent the most comprehensive comparison of the soot formation chemistry and particle growth attempted to date for diffusion flame conditions. The results are quite encouraging and continued interaction between the Penn State and University of California efforts is planned. A more detailed discussion of these results is contained in Appendix B.

3.3 Laser-Induced Incandescence Measurements of Soot Volume Fraction

Laser-induced incandescence has been used to obtain spatially-resolved measurements of soot volume fraction in a laminar diffusion flame, in which comparisons with laser scattering/extinction

data yield excellent agreement. In addition, the laser-induced incandescence signal is observed to involve a rapid rise in intensity followed by a relatively long (ca. 600 ns) decay period subsequent to the laser pulse, while the effect of laser fluence is manifest in non-linear and near-saturated response of the laser-induced incandescence signal with the transition occurring at a laser fluence of approximately 1.2×10^8 W/cm^2. Spectral response of the laser-induced incandescence involves a continuous spectrum in the visible wavelength range due to the blackbody nature of the emission. Simultaneous measurements of laser-induced incandescence and light-scattering yield encouraging results concerning the mean soot particle diameter and number concentration. Thus, laser-induced incandescence can be used as an instantaneous, spatially-resolved diagnostic of soot volume fraction without the need for the conventional line-of-sight laser extinction method, while potential applications in two-dimensional imaging and simultaneous measurements of laser-induced incandescence and light-scattering to generate a complete soot property characterization are significant. These results are presented in detail in Appendix C.

In addition to the results obtained in the laminar flame, recent work has demonstrated that similar capabilities to determined soot volume fraction in Diesel engines, droplet wakes and turbulent diffusion flames. The development of the laser-induced technique, therefore, is a significant new contribution to the array of laser-based diagnostics available for combustion measurements.

4.0 Conclusions

The major conclusions of studies undertaken during the past contract year are:

1. Soot particle surface growth terminates because of the depletion of the hydrocarbon species responsible for surface reactions which add mass to the particle. In particular, the measurements of acetylene and benzene clearly show these species decrease to trace concentration levels at the peak of the soot volume fraction location. Additional measurements using gas chromatography analysis have provided additional species concentration information and allowed an estimate of the accuracy and precision of the measurements. The availability of such an estimate was viewed as critical to meaningful comparison with soot chemistry model predictions.
2. Comparisons with results describing the aging process, which soot particles have been observed to experience under premixed flame conditions, show that this mechanism has only a small contribution to the reduction in the surface growth rate for these laminar flame conditions.
3. A current detailed model of soot formation in laminar diffusion flames was shown to be capable of reproducing the major gas phase species and soot particle fields reasonably well

(i.e. to within a factor of two). Better agreement appears possible with further refinements in the model. Of particular note is that both measurement and prediction show that radical species in these soot laden diffusion flames are far from equilibrium. This observation is critical to the development of appropriate combustion models for soot laden flows.

4. A novel quantitative laser diagnostic approach has been developed and applied to the measurement of soot volume fraction in laminar diffusion flames based laser-induced incandescence. This diagnostic approach has been validated using well known soot particle measurements previously obtained in laminar diffusion flames. The technique has recently been extended to turbulent flame, droplet burning and Diesel engine experiments.

5.0. References

1. Santoro, R. J., "Fuel Structure and Pressure Effects on the Formation of Soot Particles in Diffusion Flames," AFOSR-TR-88-0664, 1989.

2. Quay, B., Lee, T-W, Ni, T., and Santoro, R. J., "Spatially-Resolved Measurements of Soot Volume Fraction Using Laser-Induced Incandescence,"*Combustion and Flame*," In press.

3. Puri, R. and Santoro, R. J., "The Role of Soot Particle Formation on the Production of Carbon Monoxide in Fires," *Fire Safety Science Proceedings of the Third International Symposium*, Elsevier Applied Science, London, pp. 595-604 (1991).

4. Santoro, R. J., Semerjian, H. G. and Dobbins, R. A., "Soot Particle Measurements in Diffusion Flames," *Combustion and Flame*, 52, pp. 204-218 (1983).

5. Santoro, R. J., Yeh, T. T., Horvath, J. J. and Semerjian, H. G., "The Transport and Growth of Soot Particles in Laminar Diffusion Flames," *Combustion Science and Technology*, 53, p. 89 (1987).

6. Santoro, R. J., "Fuel Molecular Structure Effects on Soot Particle Growth in Diffusion Flames," *Twentieth Fall Technical Meeting of the Eastern Section of The Combustion Institute*, Paper #19, Gaithersburg, MD, Nov. 2-5, 1987.

7. Richardson, T. F. and Santoro, R. J., "Soot Growth in Diffusion Flames Burning Fuel Mixtures," *Twenty-First Fall Technical Meeting of the Eastern Section of The Combustion Institute*, Paper #44, Clearwater Beach, FL, Dec. 5-7, 1988.

8. Santoro, R. J., "Optical Measurements of Soot Particles in Flames," *Mat. Res. Soc. Symp. Proc.*, 117, pp. 157-163 (1988).

9. Puri, R., Richardson, T. F., Santoro, R. J. and Dobbins, R. A., "Aerosol Dynamic Processes of Soot Aggregates in a Laminar Ethene Diffusion Flame," *Combustion and Flame*, 92, pp. 320-333 (1993).

10. Puri, R., Moser, M., Santoro, R. J. and Smyth, K. C., "Laser-Induced Fluorescence Measurements of OH Concentration in the Oxidation Region of Laminar, Hydrocarbon Diffusion Flames," *Twenty-Fourth Symposium (International) on Combustion*, The Combustion Institute, Pittsburgh, PA, pp. 1015-1022 (1992).

11. Frenklach, M. and Wang, H., "Detailed Modeling of Soot Particle Nucleation and Growth," *Twenty-Third Symposium (International) on Combustion,* The Combustion Institute, Pittsburgh, PA, pp. 1559-1566 (1990).

12. Smooke, M. D., Lin, P., Lam, J. K. and Long, M. B., "Computational and Experimental Study of a Laminar Axisymmetric Methane-Air Diffusion Flame," *Twenty-Third Symposium (International) on Combustion* , The Combustion Institute, Pittsburgh, PA, pp. 575-582 (1990).

13. Kennedy, I. M., Kollmann, W. and Chen, J-Y., "A Model for Soot Formation in Laminar Diffusion Flames," *Combustion and Flame*, 81, pp. 73-85 (1990).

14. Megaridis, C. M. and Dobbins, R. A., "Comparison of Soot Growth and Oxidation in Smoking and Non-Smoking Ethylene Diffusion Flames," *Combustion Science and Technology*, 66, pp. 1-16 (1989).

15. Smyth, K. C., Miller, J. H., Dorfman, R. C., Mallard, W. G. and Santoro, R. J., "Soot Inception in a Methane/Air Diffusion Flame as Characterized by Detailed Species Profiles," *Combustion and Flame*, 62, pp. 157-181 (1985).

16. Puri, R. and Santoro, R. J., "Sonic Probe Sampling in Particle Laden Combustion Flows," *Twenty-Third Fall Technical Meeting of the Eastern Section of The Combustion Institute*, Orlando, FL, Dec. 3-5, 1990.

17. Honnery, D. R and Kent, J. H. , "Soot Formation in Long Ethylene Diffusion Flames," *Combustion and Flame*, 82, p. 426 (1990).

18. Kent, J. H. and Honnery, D. R., "Soot Formation Rates in Diffusion Flames - A Unifying Trend," *Combustion Science and Technology*, 75, p. 169 (1991).

6.0 Publications

1. Santoro, R. J. and Richardson, T. F., "Concentration and Temperature Effects on Soot Formation in Diffusion Flames," accepted for publication by Springer Verlag in *Mechanisms and Models of Soot Formation* (in press).

2. Puri, R., Richardson, T. F., Santoro, R. J. and Dobbins, R. A., "Aerosol Dynamic Processes of Soot Aggregates in a Laminar Ethene Diffusion Flame," *Combustion and Flame*, 92, pp. 320-333 (1993).

3. Quay, B., Lee, T-W, Ni, T. and Santoro, R. J., "Spatially-Resolved Measurements of Soot Volume Fraction Using Laser-Induced Incandescence,"*Combustion and Flame*," In press.

4. Rapp, D. C. and Santoro, R. J., "Growth Species and Soot Growth in a Laminar Diffusion Flame," Paper #WSS/CI 94-052, 1994 Spring Meeting of the Western States Section of the Combustion Institute, University of California at Davis, Davis, CA, March 21 and 22, 1994.

7.0 Meetings and Presentations

1. Lee, W., Richardson, T. F. and Santoro, R. J., "The Effects of Operating Pressure on soot Formation in Laminar Diffusion Flames," Paper #100, 1993 Joint Technical Meeting of the Central and Eastern States Sections of the Combustion Institute, New Orleans, LA, March 15-17, 1993.

2. Rapp, D. C. and Santoro, R. J., "Measurements of Soot Growth Species Concentration in Diffusion Flames," Chemical and Physical Processes in Combustion, 1993 Technical Meeting of the Eastern States Section of the Combustion Institute, Princeton University, Princeton, NJ, October 25-27, 1993, pp. 370-373.

3. Quay B., Lee T-W., and Santoro, R. J., "Spatially-Resolved Measurements of Soot Volume Fraction Using Laser-Induced Incandescence," Chemical and Physical Processes in Combustion, 1993 Technical Meeting of the Eastern States Section of the Combustion Institute, Princeton University, Princeton, NJ, October 25-27, 1993, pp. 386-389.

8.0 Participating Professionals

Dr. Robert J. Santoro, Professor of Mechanical Engineering
Dr. Tuqiang Ni, Research Associate
Dr. Tae-Woo Lee, Research Associate (Currently Assistant Professor, Arizona State University)
Dr. Rahul Puri, Graduate Student and Research Associate, Department of Mechanical Engineering (Ph.D. 9/92, currently employed at Allison Gas Turbine)
Dr. Thomas Richardson, Graduate Student, Department of Mechanical Engineering (Ph.D. 5/93, currently employed at Allison Gas Turbine).
Mr. Darrell Rapp, Graduate Student (AFRAPT), Department of Mechanical Engineering (Ph.D. expected 12/94).
Mr. Bryan Quay, Graduate Student (ASSERT), Department of Mechanical Engineering (Ph.D. expected 6/96).
Mr. Daniel Boone, Technician

9.0 Interactions

A number of researchers have directly used the extensive data set developed as part of this work to compare with or extend their own research. Some of those who have been directly provided data include:

Professor R. A. Dobbins, Brown University, Providence, RI
Dr. R. Hall, United Technologies Research Center, East Hartford, Ct
Dr. R. Davis, the National Institute of Standards and Technology, Gaithersburg, MD
Dr. P. Solomon, Advanced Fuel Research, Inc., East Hartford, CT
Dr. I. Kennedy, University of California, Davis, CA
Drs. C. Merkle and S. Turns, The Pennsylvania State University, University Park, PA
Dr. H. Mongia, Allison Gas Turbine Division-GM, Indianapolis, IN and General Electric, Aircraft Engines Division, Cincinnati, OH
Dr. K. Smyth, National Institute of Standard and Technology, Gaithersburg, MD
Dr. G. Mulholland, National Institute of Standards and Technology, Gaithersburg, MD
Prof. L. Pfefferle, Yale University, New Haven CT

In addition to the interactions resulting from interest in soot particle data, there have been interactions with researchers on particle diagnostic problems. In some cases this has resulted in direct visits to particular laboratories to assist in solving these problems. These interactions include:

Dr. M. Zachariah, The National Institute of Standards and Technology, Gaithersburg, MD
Dr. Valerie Lyons, NASA-Lewis Research Center, Cleveland, OH
Dr. Alan Scaroni, Penn State University, University Park, PA
Dr. Randy Van derWaal, NASA Lewis Research Center, Cleveland, OH

Several other interactions have also occurred through a general interest in the work supported by AFOSR with:

Columbian Chemical Company, Monroe, LA
Cummins Engine Company, Columbus, IN
E. I. DuPont De Nemours, Wilmington, De
Eastman Kodak, Rochester, NY
Allison Gas Turbine Division, Indianapolis, IN
General Electric, Aircraft Engine Division, Cincinnati, OH
Lubrizol, Wickliffe, OH

DuPont is currently supporting work on titanium dioxide particle formation as a direct result of the AFOSR research program. A student, Peter Strakey, has spent two summers with DuPont exchanging expertise and technology developed as part of this research.

Lubrizol has initiated a grant with our laboratory to examine the surface reactivity effects of soot particles on lubricants. This work complements an AASERT grant associated with this current AFOSR contract. A student, Mr. Chris Chandler, is supported on this project and works closely with Mr. Bryan Quay, as well as with personnel at Lubrizol.

Recent work with Allison Gas Turbine Division involving the incorporation of a revised soot model in their gas turbine combustion codes also occurred as a result of the present work. Mr Darrell Rapp, who is an AFRAPT participant, has spent two summers working at Allison on the implementation of that model. This work is an attempt to directly transfer the results of our work to industry. Additionally, two former PH. D. students associated with the present contract are now permanent employees of Allison and work on gas turbine related problems.

We have also previously participated by invitation in two international workshops on soot formation:

"Current Problems in Soot Formation During Combustion,: sponsored by The Commission on Condensation Phenomena of the Academy of Science, held in Gottingen, Germany, March 20-30, 1989.

"Mechanisms and Models of Soot Formation--An International Workshop," sponsored by Volkswagen, Heidelberg, Germany, September 29 - October 2, 1991.

Appendix A: Growth Species and Soot Surface Growth in a Laminar Diffusion Flame

by

D. C. Rapp and R. J. Santoro

Presented at the 1994 Spring Meeting of the Western States Section of the Combustion Institute, University of California at Davis, Davis, CA, Paper # WSS/CI 94-052, March 21 and 22, 1994

Growth Species and Soot Surface Growth in a Laminar Diffusion Flame

D.C. Rapp and R.J. Santoro

Propulsion Engineering Research Center
and
Department of Mechanical Engineering
The Pennsylvania State University
University Park, PA 16802-2320

Paper # WSS/CI 94-052
Presented at
1994 Spring Meeting
Western States Section/The Combustion Institute
University of California at Davis
Davis, CA 95616

March 21 and 22, 1994

PENNSTATE

GROWTH SPECIES AND SOOT SURFACE GROWTH IN A LAMINAR DIFFUSION FLAME

D.C. Rapp and R.J. Santoro
Propulsion Engineering Research Center
and
Department of Mechanical Engineering
The Pennsylvania State University
University Park, PA 16802-2320

ABSTRACT

Newly added measurements of the spatial distribution of species concentrations have been integrated with previous measurements to establish the mechanism controlling the cessation of soot surface growth in a laminar diffusion flame. In particular, the measurements of C_2H_2 and other hydrocarbons have revealed that soot surface growth ceases due to the depletion of hydrocarbons and not due to the loss of soot particle reactivity. This observation is in agreement with recent work by Honnery and Kent, who have shown that in long laminar diffusion flames, soot growth can be extended to very long residence times.

INTRODUCTION

Understanding of the evolution of soot particles in combustion systems has been the object of study for a wide variety of situations. Although studies conducted in practical devices, such as gas turbine combustors or Diesel engines, have yielded much useful engineering insight, fundamental understanding of soot formation and destruction has been typically gleaned from simpler flame studies. Soot formation in premixed flames have been studied quite extensively at low pressure by Howard and coworkers, (Bittner and Howard 1981; Westmoreland et al. 1989) and Bockhorn and coworkers (Bockhorn et al. 1983; Wieschnowsky et al. 1988), and at atmospheric pressure by Harris and coworkers (Harris and Weiner 1983; Harris and Weiner 1985; Harris 1990). Many of these experimental and numerical studies of soot formation (Harris et al. 1986; Frenklach and Wang 1990) involve flat flame burners which have provided insight into the evolution of the soot aerosol from inception through growth to oxidation. However, since many practical applications involve non-premixed conditions, it is important to study the soot formation processes under conditions where diffusive and mixing processes control the reaction rate (high Damköhler Number). Therefore, when focusing on fundamental soot phenomenon it is important to select as simple an environment as possible while retaining the major characteristics of diffusion flames. Though all practical combustion devices can have turbulence to very high levels, it is more tractable to study soot formation

under laminar conditions where the complexities of turbulence do not complicate the primary object of study.

Among the simplest laminar diffusion flames which contains many characteristics of practical combustors is an axisymmetric system of gaseous fuel issuing from a tube with a larger flow of air surrounding it. The experimental setup is straightforward and the flames are quite stable.

In the present experiment, the burner configuration and dimensions are identical to that used by previous researchers to acquire a significant set of data on flow variables (temperature and velocity) (Santoro et al. 1987) as well as data on the soot aerosol (volume fraction, number density and particle diameter) (Santoro et al. 1983). Recently, hydroxyl (OH) radical mole fractions have been determined using laser-induced fluorescence (Puri et al. 1992) and fluorescence from polycyclic aromatic hydrocarbons have been examined (Richardson 1993). Due to this extensive database, researchers involved in the numerical modeling of the soot formation and/or chemical kinetics in diffusion flames have endeavored to model this system (Kennedy et al. 1990; Kennedy et al. 1994) or similar systems (Mitchell et al. 1980; Smooke et al. 1990).

The present work expands on this set of data for a laminar diffusion flame burning C_2H_4 in air. The information to be added to the existing measurements involve the spatial distribution of the molecular species in the flame. When combined with the velocity measurements, knowledge of the environment surrounding the soot particles on a temporal basis is gained. The following discussion will pursue a more sophisticated analysis of the data than previously possible in the surface growth region.

In order to determine the distribution of molecular species throughout the flame, a method of measuring the concentrations is necessary. Although several non intrusive laser-based techniques exist for species measurements (e.g. LIF, absorption, CARS, Raman) many are limited in the number of species that can be quantitatively measured. Furthermore, when soot particles are present interference with the measurements can make these procedures difficult if not impossible to accomplish (Eckbreth et al. 1979). Therefore, intrusive probes, which have been used for many years, will be used to extract gas samples for on-line or later batch analysis.

EXPERIMENTAL

A laminar ethene/air diffusion flame was established on a coannular burner similar in design to that used in previous studies (Santoro et al. 1983) and only a brief description will be given

here. This burner is shown in Figure 1 and consists of a 1.11 cm diameter brass fuel tube surrounded by a 10.2 cm diameter air annulus. A brass cylindrical chimney was used to shield the flame from laboratory air currents with access for sampling provided by slots machined in the chimney wall. The ethene and air flow rates were 3.85 cm^3/s and 713 cm^3/s respectively, which were measured with calibrated rotameters. Ethene with a stated purity of 99.5% was used, while filtered and dried air was supplied by an in-house compressor. These conditions replicate those of Santoro and coworkers (Santoro et al. 1983; Santoro and Semerjian 1984; Santoro et al. 1987) so that the current and previous measurements can be brought together synergistically.

Radial profile measurements of species concentrations have been obtained throughout the soot growth region of the flame using an intrusive quartz microprobe sampling approach. Quartz microprobes have been used in many studies to perform the extraction of gas samples from premixed flames (Fristrom et al. 1957; Bockhorn et al. 1983) and diffusion flames (Smith and Gordon 1956; Mitchell 1975; Crowhurst and Simmons 1985; Smyth et al. 1985; Puri 1992). Until recently their use has been limited to regions where the soot volume fraction is low to avoid clogging the small probe orifice (≈100 μm). A variation of the standard quartz microprobe design, referred to as an Electro-Mechanical Sonic (EMS) probe (Puri 1992) is shown in figure 2 and enables sampling in flame regions where volume fractions are on the order of 10^{-5}.

The EMS probe utilizes a fiber that extends through the orifice and is attached to a solenoid core with springs on either side of the core. A solenoid is placed around the outside of the quartz tube and the current to the solenoid is interrupted at about 30 Hz, providing for constant oscillatory motion of the fiber within the orifice, thus keeping an annular region open for gas sampling. The fiber is ≈125 μm in diameter and is made from sapphire, while the orifice diameter is ≈190 μm. The annular sampling region has an area equivalent to a ≈130 μm diameter orifice.

In addition to the EMS probe, it is also necessary to use a rapid insertion procedure similar to that originally described by Kent and Wagner (1984) for use with thermocouples in flames with high soot concentrations. This procedure involves alternately removing the probe tip from the sample location in the flame to a lean high temperature region where soot will burn from the tip leaving a clean orifice before moving to the next sample location.

SPECIES ANALYSIS

Analysis of the collected gas samples was done using a mass spectrometer (MS) and a gas chromatograph (GC). The use of these two techniques allowed an independent verification of the concentration profile measurements as well as providing specific species measurement capability as described below.

Mass Spectrometer: The mass spectrometer employed an Extrel model 7-324-9 quadrupole mass filter with mass range of 1-500 u for separation of ions and an electron multiplier for detection. A computer controlled the ionizer, the mass filter and the burner position while the signal was recorded by the computer through an A/D converter.

As shown in figure 3, a staged vacuum pumping system was employed. The EMS probe was used to continuously extract sample from the flame. The pressure in the small vacuum chamber was on the order of 1 Torr. The orifice of a second quartz probe was situated in the exit stream of the EMS probe and allowed a small amount of the flame sample gas to pass into the high vacuum chamber where the pressure was on the order of 10^{-6} Torr. The secondary probe discharges the molecular sample into the electron impact ionizer which has tungsten filaments. The resultant ions were extracted, focused and accelerated into the mass filter for separation. The mass filter was operated in single ion mode and the ionizer was operated at 20 eV or less to reduce molecular fragmentation.

The calibration method for the MS follows the procedure given by Ermolin et al. (1982) as shown in equation (1) where F_i and S_i are the calibration factor and signal intensity respectively for species i. This method is mathematically similar to Bittner (1981) and Crowhurst and Simmons (1985). The method relies on the signal response relative to other species remaining constant. That is, for a given mixture the ratio of the signals due to two gases will always be the same and, therefore, is independent of variations in mass flow through the orifice due to orifice clogging or variations in density. Secondly, this method assumes that the species measured constitute all of the gases present which are normalized to a mole fraction of one.

$$X_i = \frac{F_i S_i}{\sum F_j S_j} \qquad (1)$$

Determination of the calibration factors were performed with a gas of known mole fraction of a given species flowing through the burner fuel tube so that any biases relating to the sampling procedure or MS characteristics are included in the calibration factor, F_i. Calibrations for N_2, O_2, and Ar used air as the standard gas. Calibration of H_2O employed a N_2 stream saturated

with H_2O vapor. Other species used commercial calibrated mixtures or calibrated flowmeters to mix pure gases in the appropriate ratios. The molecular species measured directly by the MS are N_2/CO, O_2, C_2H_4, H_2O, CO_2, C_2H_2, H_2, CH_4, and Ar.

One limitation of the use of a MS in the present study is the coincidence of C_2H_4, N_2 and CO at mass 28. For C_2H_4, the fragment at mass 27 was used as an independent measurement. Calibration of C_2H_4 at both masses 27 and 28 was necessary so that the signal contribution of C_2H_4 at mass 28 could be subtracted from the mass 28 signal. C_2H_4 was similarly calibrated and subtracted at mass 26 where C_2H_2 was measured.

Furthermore, it is not possible to determine the signal of N_2 or CO independently with the MS. Therefore, the analysis is performed as though there was no CO present. Since CO, as determined by the GC measurements, can yield mole fractions of close to 0.10 at some locations in the flame, this approach will overpredict the N_2 by somewhat more than the measured CO concentration due to the greater sensitivity of the MS to CO and reduce the mole fractions of other species slightly due to the normalization procedure shown in equation (1).

Gas Chromatograph: A Hewlett-Packard 5890 GC employed Porapak Q and Porapak S columns coupled with a molecular sieve (5Å) for species separation using a column sequence reversal technique and temperature programming. A dry ice bath was used to extract H_2O from the sample to simplify storage requirements. A Thermal Conductivity Detector (TCD) was used for detection of all non-hydrocarbons (N_2, O_2/Ar, CO, and CO_2). A Flame Ionization Detector (FID) was used for detection of hydrocarbons in small concentrations. For concentrations of hydrocarbons which were beyond the linear range of the FID, the TCD was used. A signal integrator is attached to each detector for recording of the chromatogram.

Since the gas chromatograph requires the sample to be at atmospheric pressure and the EMS probe collects samples at low pressure, a method was devised to collect a sample in a cylinder and compress it with a piston for storage in a multiloop sample storage system (Puri 1992). The schematic of this compression apparatus is shown in Figure 4. Each sample is stored in a 10 cm^3 loop at two atmospheres. After fifteen samples are collected in separate storage loops, the sample storage system is connected to the GC and each sample is analyzed sequentially. One of the GC signal integrators controls the GC and the multiposition valve connected to the sample storage system.

Calibration of the GC was primarily done using commercially available gas mixtures with accuracy of ±2%. The GC was also calibrated for fuel species concentrations much greater than

that available commercially using laboratory prepared mixtures. The GC signal integrators used with the TCD and FID were able to perform multi-level calibrations for species which spanned large ranges in concentrations. The molecular species calibrated and measured directly with the GC are N_2, O_2/Ar, C_2H_4, CO_2, C_2H_2 , CO, CH_4, and C_2H_6. The columns cannot separate O_2 and Ar.

For optimal detection of species with the TCD, helium was used as the carrier gas. Since detection depends on the difference in thermal conductivities, measurements of molecular hydrogen are problematic. In addition, the samples were dried prior to storage, thus, the H_2O concentration is obtained by a hydrogen atom balance approach developed by Puri (1992), which assumes all species diffuse similarly. This method calculates how much hydrogen should be present from the amount of carbon present (from measurements of carbon containing species) and the carbon to hydrogen ratio in the fuel. The amount of H_2O is then calculated from the difference between this calculated amount of hydrogen and the actual hydrogen present in the hydrogen containing species which have been measured. Finally the dry measurements were normalized with the calculated H_2O concentration assuming the measured species mole fractions sum to one. This method overestimates the concentration of H_2O since it ignores molecular hydrogen, but the mole fractions are unaffected since both species contain two hydrogen atoms.

To determine the centerline position, the MS data was used since these data were obtained across the entire diameter of the flame and were generally symmetrical. The primary method was to assign the two locations where fuel and oxygen disappear to the same radius. At higher axial positions when the fuel was almost fully consumed, either the C_2H_2 or H_2 profile was used in a similar manner or directly to center the data. The radial position of the data obtained from the GC analysis, which was obtained for only one-half of the flame diameter because of sample storage limitations, was determined by setting the position where fuel and oxygen disappear to match the MS measurements.

Measurements using the above instrumentation will be combined with the temperature (fine wire thermocouples), velocity (Laser Doppler Anemometer) and soot aerosol information (laser extinction and scattering) which have been published earlier for this same flame (Santoro et al. 1983; Santoro and Semerjian 1984; Santoro et al. 1987). The experimental details of those measurements are not discussed here.

RESULTS

Spatially resolved measurements of molecular species have been determined throughout the region of the flame where soot undergoes growth processes. Radial measurements at 7, 10, 20, 30, 40 and 50 mm above the burner exit have been taken with both the MS and GC. Measurements were taken at 0.5 mm radial steps with the MS, while the GC measurements were limited to 15 samples per experiment, so samples were taken judiciously to resolve the important features in the flame. For the species measured by both instruments the results generally agreed to ±20% or better with the exception of acetylene which displayed a somewhat larger difference for the two measurement techniques. However, due to the subtraction procedure for calculating the mole fraction of C_2H_2, the measurements of acetylene generally agreed within the measurement errors.

As an illustration of the spatial distribution of the mole fractions of C_2H_4 and C_2H_2 is shown in figure 5 for several heights in the flame for both the MS and GC. Note that the rapid consumption of the fuel results in a peak mole fraction of less than 0.01 at 30 mm above the burner outlet.

Examination of the radial profile for the C_2H_2 mole fraction at the 7 and 10 mm heights indicates the maximum value occurs at a radial position different from the centerline. This result implies that the highest production rates for C_2H_2 occurs in an annular region approximately 4-5 mm in radius. The quantities of C_2H_2 at the centerline indicate some production of C_2H_2 throughout the central region of the flame as well. In fact, the increase in the maximum mole fraction continues through to the 20 mm axial measurement location where the maximum concentration is observed to occur at the centerline and indicates net formation of C_2H_2 up to this height. After the fuel concentration approaches zero near the 30 mm height the C_2H_2 peak mole fraction decreases by a factor of about four by 40 mm to 0.01 and further decreases by a factor of about ten by 50 mm to 0.001 as reactions proceed. Concentrations at the 40 mm height, which include a small amount of measured hydrocarbons remaining to be oxidized, coincides with the peak in the integrated soot volume fraction in this flame. At this height, soot represents 14% of the total carbon flow rate in the flame (Santoro et al. 1987). The major gaseous species remaining to be oxidized at this height are CO, H_2, and C_2H_2 with peak mole fractions of approximately 0.07, 0.02, and 0.01 respectively.

In addition to C_2H_2, which is argued to be a major surface growth species, measurements of diacetylene (C_4H_2) and benzene (C_6H_6) were also obtained with the MS. Calibrations for these species were not available so only the relative signal intensities will be discussed. Figure 6

shows plots of the signal profiles for C_4H_2 and C_6H_6 for several axial positions in the ethene flame. The C_4H_2 profiles indicate net production is occurring from the 7 to 20 mm axial locations. The signal to noise limitation on these small signals makes it difficult to definitively state that an annular region is favored, but the wide spatial distribution of these species indicates a broad range of radial positions where formation occurs. Between the 20 and 30 mm axial locations, the magnitude of the peak signal intensity decreases somewhat while the profile becomes narrower. This suggests that production of C_4H_2 may still occur in the center region of the flame followed by subsequent diffusion to the flame front with the consumption rate slightly exceeding the production rate of C_4H_2. Above the 30 mm axial location production rapidly diminishes as compared to consumption and the C_4H_2 concentration decreases significantly by 40 mm. The benzene signals show a somewhat different evolution. Although net production is also observed over the region between the 7 mm and 20 mm axial locations, no height has a distinctive peak intensity away from the centerline. Thus, benzene is rapidly formed throughout the center region of the ethene flame in contrast to C_2H_2 and to a lesser extent C_4H_2 which initially favor the annular region. The peak signal intensity of C_6H_6 increases significantly by the 20 mm axial location as compared to the 7 mm axial location, but then decreases by almost one-third between the 20 and 30 mm heights. This implies a smaller region where conditions favor net production of C_6H_6.

The GC measurements indicate the presence of additional hydrocarbons which were not identified in the present study. The spatial development of the concentrations of these species is similar to that reported for C_4H_2 and C_6H_6 as determined by the MS. That is, the concentrations increase approximately through the 20 or 30 mm axial locations and then decrease in concentration and spatial extent with increasing height. At the lower axial positions, some of these species produce profiles with a maximum concentration in the annular region.

DISCUSSION

One question which arises in both premixed and diffusion flames with respect to soot formation pertains to the cessation of growth of soot particles in the flame. In premixed flames, it has been found that significant quantities of C_2H_2 and other hydrocarbons persist into the post flame region (Harris and Weiner 1983; Bockhorn et al. 1984). It is in this region that particle inception occurs and the surface growth reactions proceed. Furthermore, the rate of these surface reactions decreases with time while the hydrocarbon concentrations do not change appreciably. This experimental result has been used to argue that the reactivity of the

particles decreases with time and has been discussed by others (Dasch 1985; Woods and Haynes 1991).

In diffusion flames little information has been available about the chemical environment surrounding the soot particles as they traverse the flame. The combination of the previous measurements of Santoro and coworkers (Santoro et al. 1983; Santoro and Semerjian 1984; Santoro et al. 1987) with the spatial species measurements allows analysis which can help to elucidate information about some of the chemistry involved.

The following analysis integrates the previous measurements of flowfield and soot with the molecular species information now available. From the velocity measurements, soot particle paths have been determined and, thus, the detailed temporal evolution of soot particle growth can be obtained (Santoro et al. 1983; Santoro and Semerjian 1984; Santoro et al. 1987). In the present case, the soot growth process will be examined in relationship to the concentration field of C_2H_2 since it has been argued to be the primary growth species in premixed flames (Harris and Weiner 1983). In examining this process, three particle paths will be considered. One particle path passes through the maximum observed local soot volume fraction. A second considers the centerline of the flame. The third is midway between these two particle paths and is designated the middle particle path. For the two paths away from the centerline, the appropriate data from both sides of the flame have been averaged and then the analysis performed. This is due to the symmetric nature of the flame and the arbitrary choice which would be necessary when combining the two sets of data.

Figure 7 shows the local soot volume fraction, f_v, and the C_2H_2 mole fraction as a function of time along each of these particle paths. The trends on these three particle paths are typical of the evolution observed along other particle paths in the flame. The important characteristic is that the soot volume fraction achieves a maximum at the same axial location where the C_2H_2 concentration approaches zero. The qualitative measurements of C_4H_2 and C_6H_6 with the MS and the unidentified hydrocarbon measurements from the GC indicate a similar depletion at the same height. Thus, it is argued that the depletion of hydrocarbons available for soot particle growth is the reason for particle growth ceasing. The present measurements for these ethene/air diffusion flames show a different mechanism for the cessation of soot growth is operative as compared to premixed flames.

The underlying phenomenon of this depletion mechanism presented above can be approached in two ways. These are best explained by looking at a general rate equation for soot formation in equation (2)

$$\frac{df_v}{dt} = Growth - Oxidation \qquad (2)$$

It is first important to notice that when the volume fraction is measured, it is the net rate of growth and oxidation which is determined. So obviously, a transition from net soot formation to net soot destruction occurs when the rate of the oxidation reactions becomes comparable to the rate of the growth reactions. This transition corresponds to the location of the maximum soot volume fraction along a given particle path.

When one proceeds to examine why such a transition occurs, it is necessary to consider the structure of the flame and the specifics of the soot growth process. In a laminar diffusion flame, fuel is transformed into products as one proceeds higher in the flame. The data from the present study shows that beyond the 30 mm height above the burner exit, all measured hydrocarbon concentrations decrease dramatically. This decrease in hydrocarbons available for soot growth will slow the growth reactions since this rate would generally be dependent upon the concentration of species participating in surface growth reactions.

The decrease in hydrocarbons is followed by a corresponding increase in species available to participate in the oxidative reactions. Therefore, a transition occurs where the growth reactions in equation (2) decrease and the oxidation reactions increases, which yields the position of maximum local soot volume fraction along a given streamline. This corresponds to the position where the streamline has a local equivalence ratio of approximately one based on measured gaseous species.

Further evidence that supports a mechanism in laminar diffusion flames which differs from that dominant in premixed flames can be gleaned by examining the temperatures along these streamlines and using the results of Dasch (1985) and Woods and Haynes (1991) to examine the decrease in soot particle reactivity. Equation (3) expresses the decay in the reactivity of the soot surface as taken from Dasch (1985). The term k_{SG}, which was determined from Woods and Haynes, is the same term as α used by Dasch. Figure 8 shows the temperatures along the three streamlines.

$$k_{C_2H_2} \Big/ k^o_{C_2H_2} = N_s \Big/ N^o_s = \exp(-\alpha t) \qquad (3a)$$

$$\alpha = 3.5X10^7 \exp(-T_a / T) \qquad (3b)$$

While it may not be good practice to apply the above formula for reactivity decay to non isothermal flames (Haynes and Wagner 1982; Roth and Hospital 1992) there is insight to be gained by proceeding along this line of analysis. If the maximum temperature along the

streamline for the soot growth region (i.e. from initial detection of soot to the maximum soot volume fraction) is chosen, one can calculate a conservative estimate of the decrease in the soot particle reactivity along that particle path. For the three particle paths described earlier, the maximum temperatures and soot residence times are shown in Table 1. In addition, the residence time for the centerline of a C_2H_4 flame discussed by Honnery and Kent (1990) is also tabulated and is about five times longer than any of the residence times observed for the present study. The characteristic time, $1/\alpha$, for soot particle reactivity decrease is calculated using the activation temperature and expression of Dasch (1985) (see equation (3)), since the result is more conservative than that of Woods and Haynes (1991). The results will not differ appreciably since the activation temperatures differ by approximately 1%. The fraction of initial reactivity that would remain when growth ceases is also shown in Table 1.

TABLE 1 Data for calculation of particle reactivity decrease along several particle paths

Particle Path	Maximum Temperature (K)	Soot Residence Time (sec)	Characteristic Time (sec)	Fraction of Initial Reactivity
Centerline	1439	0.017	0.196	0.92
Middle	1449	0.035	0.175	0.82
Maximum	1572	0.026	0.0518	0.61
Honnery and Kent (1990)	≈1250	>0.2	2.11	0.91

The Arrhenius nature of the expression for the reactivity decrease can be expected to differ somewhat in the temperature range observed in the present diffusion flame. However, Woods and Haynes (1991) did not expect this effect to be significant.

Using the temperatures and residence times from Table 1, the fraction of the initial reactivity available is lowest, 0.61, for the particle path designated as the maximum soot volume fraction due to the higher temperature on this particle path. Furthermore, when the data from Honnery and Kent is used along the centerline of their flame, this analysis yields a fraction of initial reactivity available at the end of growth of 0.91. These values for the surface reactivity indicate that the continued growth of soot in diffusion flames to very long residence times is not in conflict with the results obtained by others in premixed flames. Furthermore, they further support the interpretation that soot surface growth in laminar diffusion flames ceases due to the depletion of gas phase reactants.

CONCLUSIONS

Newly added measurements of the spatial distribution of species concentrations have been integrated with previous measurements to establish the mechanism controlling the cessation

of soot surface growth in a laminar diffusion flame. In particular, the measurements of C_2H_2 and other hydrocarbons have revealed that soot surface growth ceases due to the depletion of hydrocarbons and not due to the loss of soot particle reactivity. This observation is in agreement with recent work by Honnery and Kent (1990), who have shown that in long laminar diffusion flames, soot growth can be extended to very long residence times.

NOMENCLATURE

α	Particle Reactivity Decrease Factor (s^{-1})
F_i	Mass Spectrometer Calibration Factor for species i (V^{-1})
f_v	Soot Volume Fraction (cm^3-soot/cm^3)
$k_{C_2H_2}$	Surface Growth Rate Constant (cm s^{-1} atm(C_2H_2)$^{-1}$)
N_s	Concentration of Active Sites (sites/cm^2)
S_i	Mass Spectrometer Signal for Species i (V)
t	Time (s)
T_a	Activation Temperature (K)
X_i	Mole Fraction of species i (-)

Superscript

o	initial value at inception

REFERENCES

Bittner, J. D. "A Molecular Beam Mass Spectrometer Study of Fuel-Rich and Sooting Benzene-Oxygen Flames." Ph. D., Massachusetts Institute of Technology, 1981.

Bittner, J. D. and J. B. Howard, "Composition Profiles and Reaction Mechanisms in a Near-Sooting Premixed Benzene/Oxygen/Argon Flame," Eighteenth Symposium (International) on Combustion, The Combustion Institute, Pittsburgh, 1981, pp. 1105-1116.

Bockhorn, H., F. Fetting, A. Heddrich, and G. Wannemacher, "Investigation of the Surface Growth of Soot in Flat Low Pressure Hydrocarbon Oxygen Flames," Twentieth Symposium (International) on Combustion, The Combustion Institute, Pittsburgh, 1984, pp. 979-988.

Bockhorn, H., F. Fetting, and H. W. Wenz, "Investigation of the Formation of High Molecular Hydrocarbons and Soot in Premixed Hydrocarbon-Oxygen Flames," Berichte der Bunsen-Gesellschaft für Physikalische Chemie 87: 1067-1073 (1983).

Crowhurst, D. and R. F. Simmons, "A Structural Study of Methane-Acetonitrile-Oxygen Diffusion Flames Diluted with Argon," Combustion and Flame 59: 167-176 (1985).

Dasch, C. J., "The Decay of Soot Surface Growth Reactivity and its Importance in Total Soot Formation," Combustion and Flame 61: 219-225 (1985).

Eckbreth, A. C., P. A. Bonczyk, and J. F. Verdieck, "Combustion Diagnostics by Laser Raman and Fluorescence Techniques," Progress in Energy and Combustion Science 5: 253-322 (1979).

Ermolin, N. E., O. P. Korobeinichev, A. G. Tereshchenko, and V. M. Fomin, "Measurement of the Concentration Profiles of Reacting Components and Temperature in an Ammonium Perchlorate Flame," Combustion, Explosion, and Shock Waves 18: 36-38 (1 1982).

Frenklach, M. and H. Wang, "Detailed Modeling of Soot Particle Nucleation and Growth," Twenty-Third Symposium (International) on Combustion, The Combustion Institute, Pittsburgh, 1990, pp. 1559-1566.

Fristrom, R. M., R. Prescott, and C. Grunfelder, "Flame Zone Studies III - Techniques for the Determination of Composition Profiles of Flame Fronts," Combustion and Flame 1: 102-113 (1957).

Harris, S. J., "Surface Growth and Soot Particle Reactivity," Combustion Science and Technology 72: 67-77 (1990).

Harris, S. J. and A. M. Weiner, "Surface Growth of Soot Particles in Premixed Ethylene/Air Flames," Combustion Science and Technology 31: 155-167 (1983).

Harris, S. J. and A. M. Weiner, "Chemical Kinetics of Soot Particle Growth," Annual Reviews in Physical Chemistry 36: 31-52 (1985).

Harris, S. J., A. M. Weiner, R. J. Blint, and J. E. M. Goldsmith, "Concentration Profiles in Rich and Sooting Ethylene Flames," Twenty-First Symposium (International) on Combustion, The Combustion Institute, Pittsburgh, 1986, pp. 1033-1045.

Haynes, B. S. and H. G. Wagner, "The Surface Growth Phenomena in Soot Formation," Zeitschrift für Physikalische Chemie Neue Folge 133: 201-213 (1982).

Honnery, D. R. and J. H. Kent, "Soot Formation in Long Ethylene Diffusion Flames," Combustion and Flame 82: 426-434 (1990).

Kennedy, I. M., W. Kollman, and J. Y. Chen, "A Model For Soot Formation in Laminar Diffusion Flames," Combustion and Flame 81: 73 (1990).

Kennedy, I. M., D. C. Rapp, R. J. Santoro, and C. Yam, "Modeling and Measurements of Soot and Species in a Laminar Diffusion Flame," Submitted to Twenty-Fifth International Symposium on Combustion.

Kent, J. H. and H. G. Wagner, "Why Do Diffusion Flames Emit Smoke?," Combustion Science and Technology 41: 245-269 (1984).

Mitchell, R. E. "Nitrogen oxide formation in laminar methane-air diffusion flames." Ph.D., Massachusetts Institute of Technology, 1975.

Mitchell, R. E., A. F. Sarofim, and L. A. Clomburg, "Experimental and Numerical Investigation of Laminar Diffusion Flames," Combustion and Flame 37: 227-244 (1980).

Puri, R. "The Interaction of Soot Particles with Carbon Monoxide in Laminar Diffusion Flames." Ph.D., The Pennsylvania State University, 1992.

Puri, R., M. Moser, R. J. Santoro, and K. C. Smyth, "Laser-Induced Fluorescence Measurements of OH Concentrations in the Oxidation Region of Laminar, Hydrocarbon Diffusion Flames," Twenty-Fourth Symposium (International) on Combustion, The Combustion Institute, Pittsburgh, 1992, pp. 1015-1022.

Richardson, T. F. "The Effects of Temperature, Fuel Concentration, and Fuel Molecular Structure on Soot Formation in Laminar Diffusion Flames." Ph.D., The Pennsylvania State University, 1993.

Roth, P. and A. Hospital, "Mass Growth and Coagulation of Soot Particles in Low Pressure Flames," Twenty-Fourth Symposium (International) on Combustion, The Combustion Institute, Pittsburgh, 1992, pp. 981-989.

Santoro, R. J. and H. G. Semerjian, "Soot Formation in Diffusion Flames: Flow Fate, Fuel Species, and Temperature Effects," Twentieth Symposium (International) on Combustion, The Combustion Institute, Pittsburgh, 1984, pp. 997-1006.

Santoro, R. J., H. G. Semerjian, and R. A. Dobbins, "Soot Particle Measurements in Diffusion Flames," Combustion and Flame 51: 203-218 (1983).

Santoro, R. J., T. T. Yeh, J. J. Horvath, and H. G. Semerjian, "The Transport and Growth of Soot Particles in Laminar Diffusion Flames," Combustion Science and Technology 53: 89-115 (1987).

Smith, S. R. and A. S. Gordon, "Studies of Diffusion Flames. I. The Methane Diffusion Flame," Journal of Physical Chemistry 60: 759-763 (1956).

Smooke, M. D., P. Lin, J. K. Lam, and M. B. Long, "Computational and Experimental Study of a Laminar Axisymmetric Methane-Air Diffusion Flame," Twenty-Third Symposium (International) on Combustion, The Combustion Institute, Pittsburgh, 1990, pp. 575-582.

Smyth, K. C., J. H. Miller, R. C. Dorfman, W. G. Mallard, and R. J. Santoro, "Soot Inception in a Methane/Air Diffusion Flame as Characterized by Detailed Species Profiles," Combustion and Flame 62: 157-181 (1985).

Westmoreland, P. R., A. M. Dean, J. B. Howard, and J. P. Longwell, "Forming Benzene in Flames by Chemically Activated Isomerization," Journal of Physical Chemistry 93: 8171-8180 (1989).

Wieschnowsky, U., H. Bockhorn, and F. Fetting., "Some New Observations Concerning the Mass Growth of Soot in Premixed Hydrocarbon-Oxygen Flames.," Twenty-Second Symposium (International) on Combustion, The Combustion Institute, Pittsburgh, 1988, pp. 343-352.

Woods, I. T. and B. S. Haynes, "Soot Surface Growth at Active Sites," Combustion and Flame 85: 523-525 (1991).

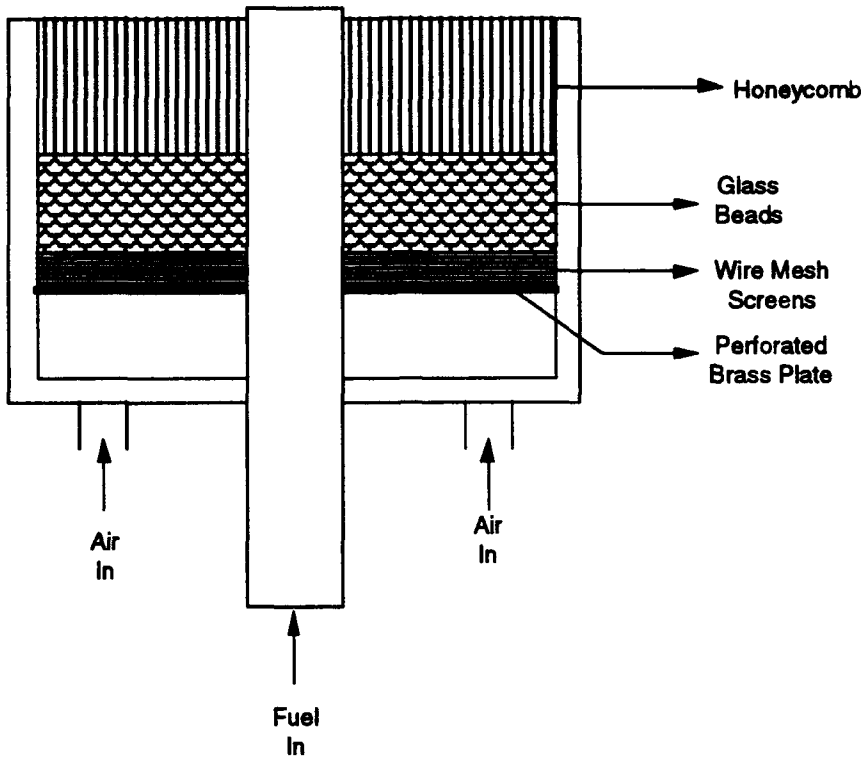

FIGURE 1 Schematic of coannular diffusion flame burner.

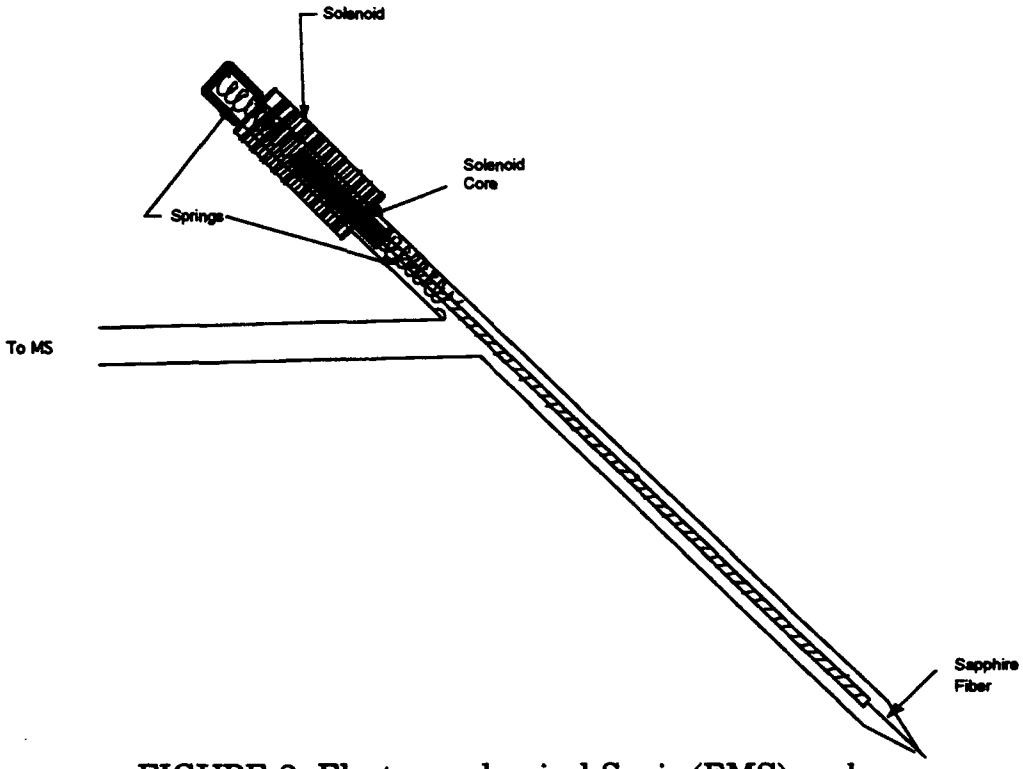

FIGURE 2 Electromechanical Sonic (EMS) probe.

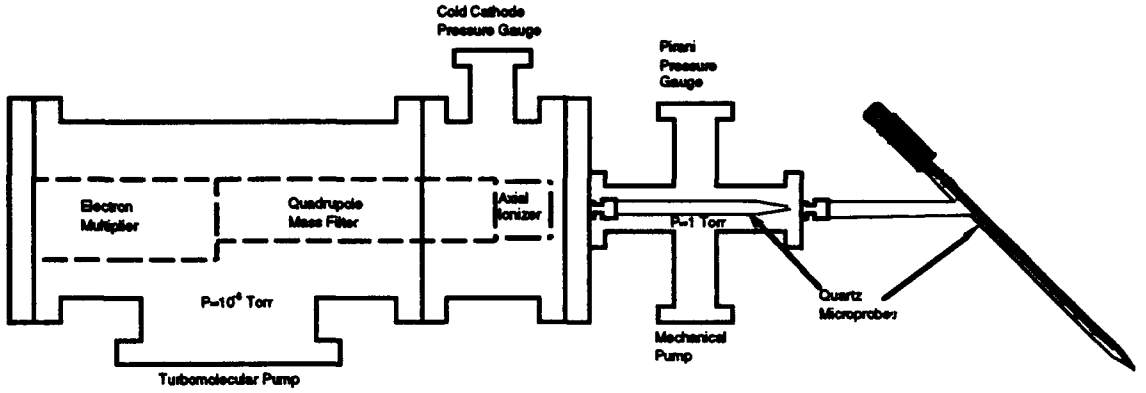

FIGURE 3 Schematic of vacuum chambers with Mass Spectrometer

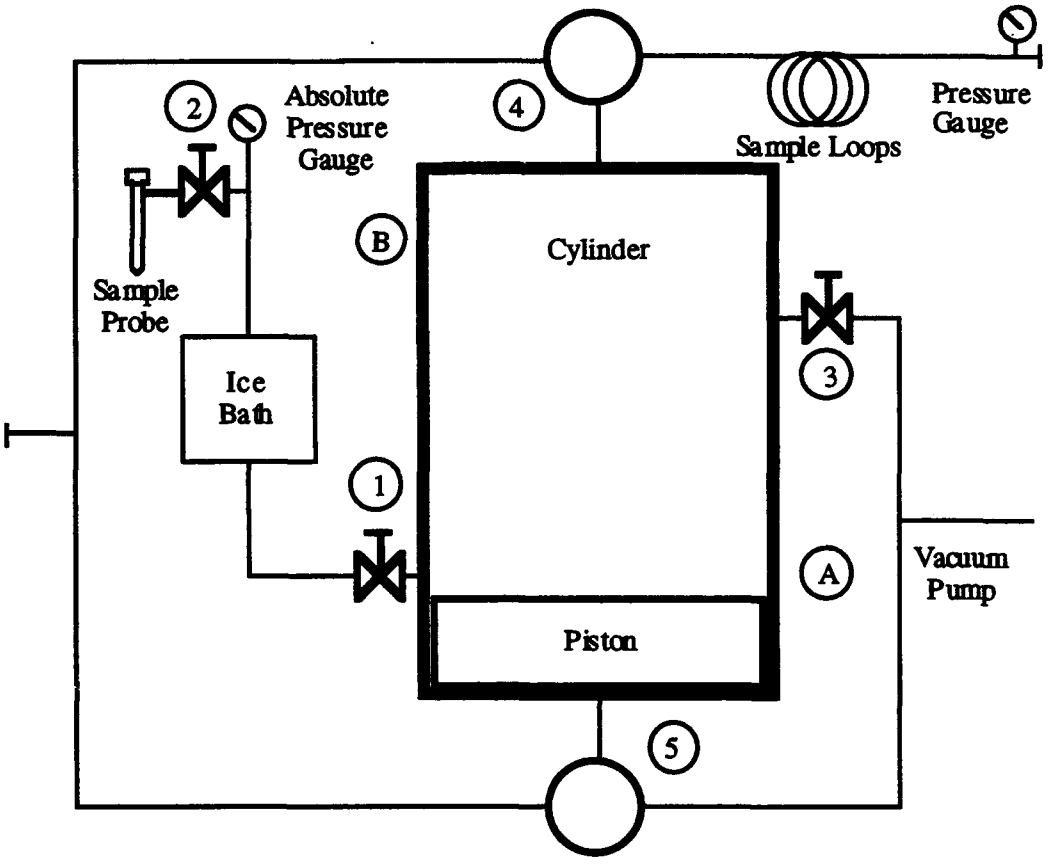

FIGURE 4 Cylinder system for compression and storage of gas sample in preparation of injection into Gas Chromatograph

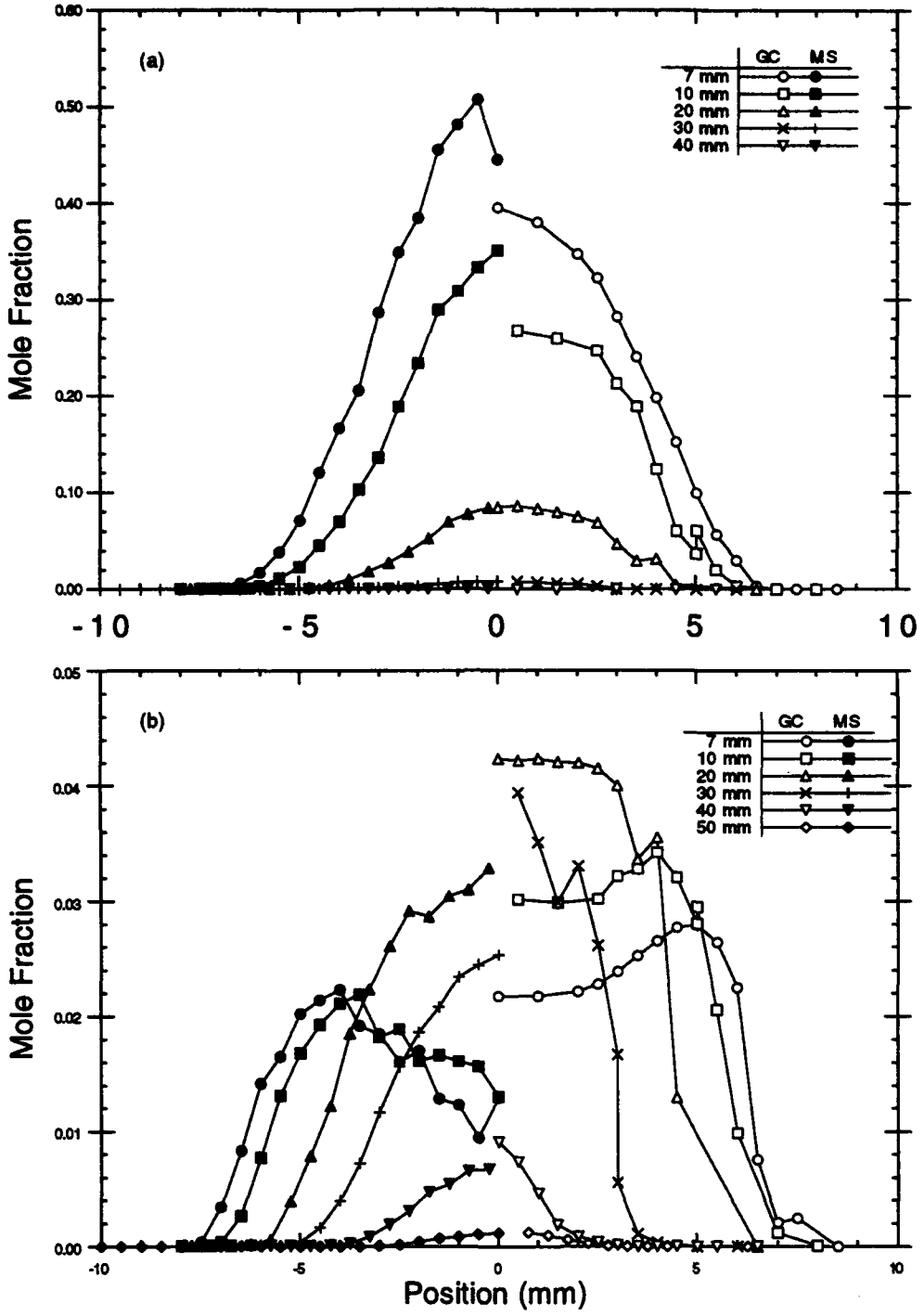

FIGURE 5 Plots of mole fraction as a function of radial position for several heights above the burner outlet (a) C_2H_4 and (b) C_2H_2

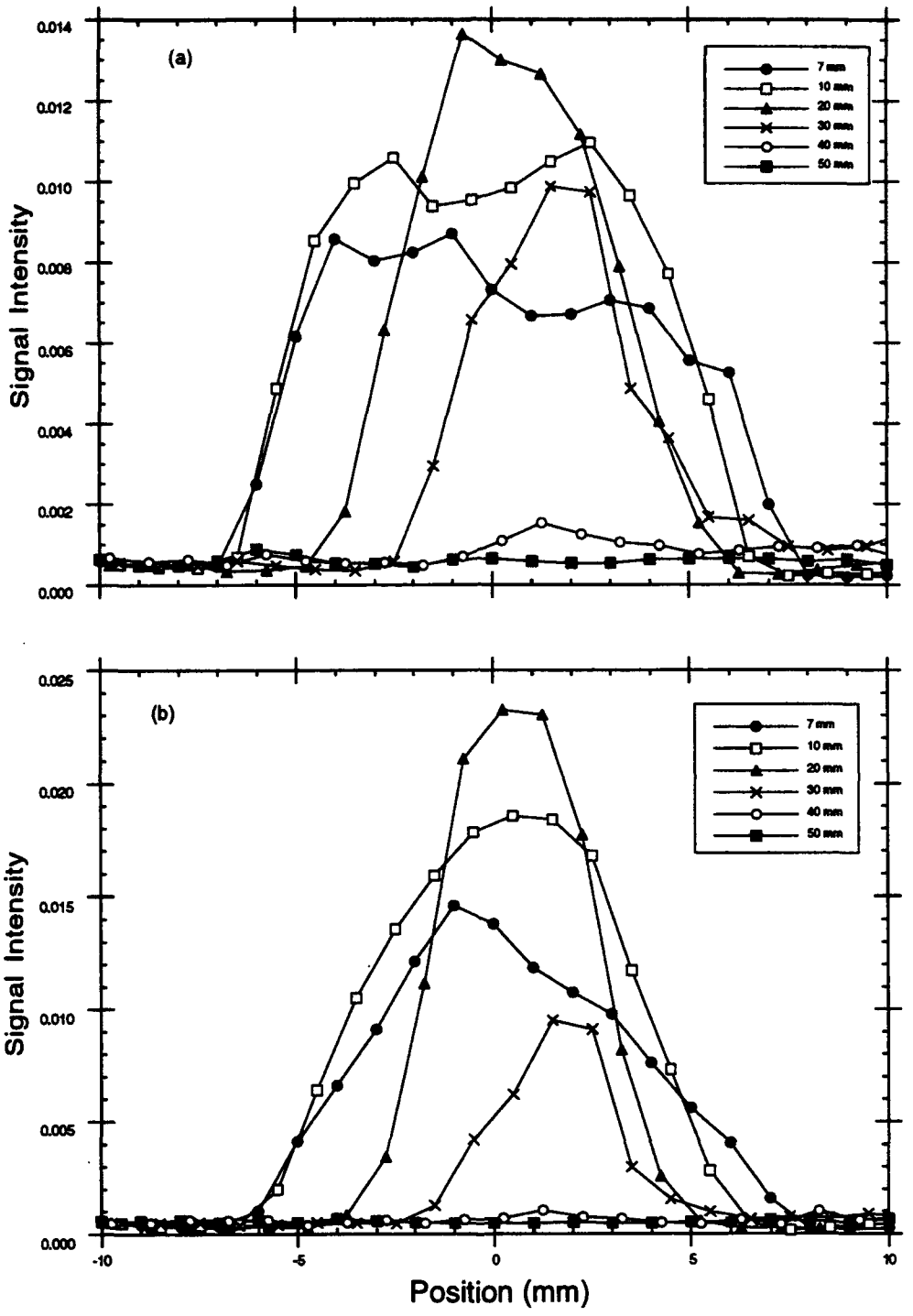

FIGURE 6 Plots of signal intensity as a function of radial position for several heights above the burner outlet (a) C_4H_2 (b) C_6H_6

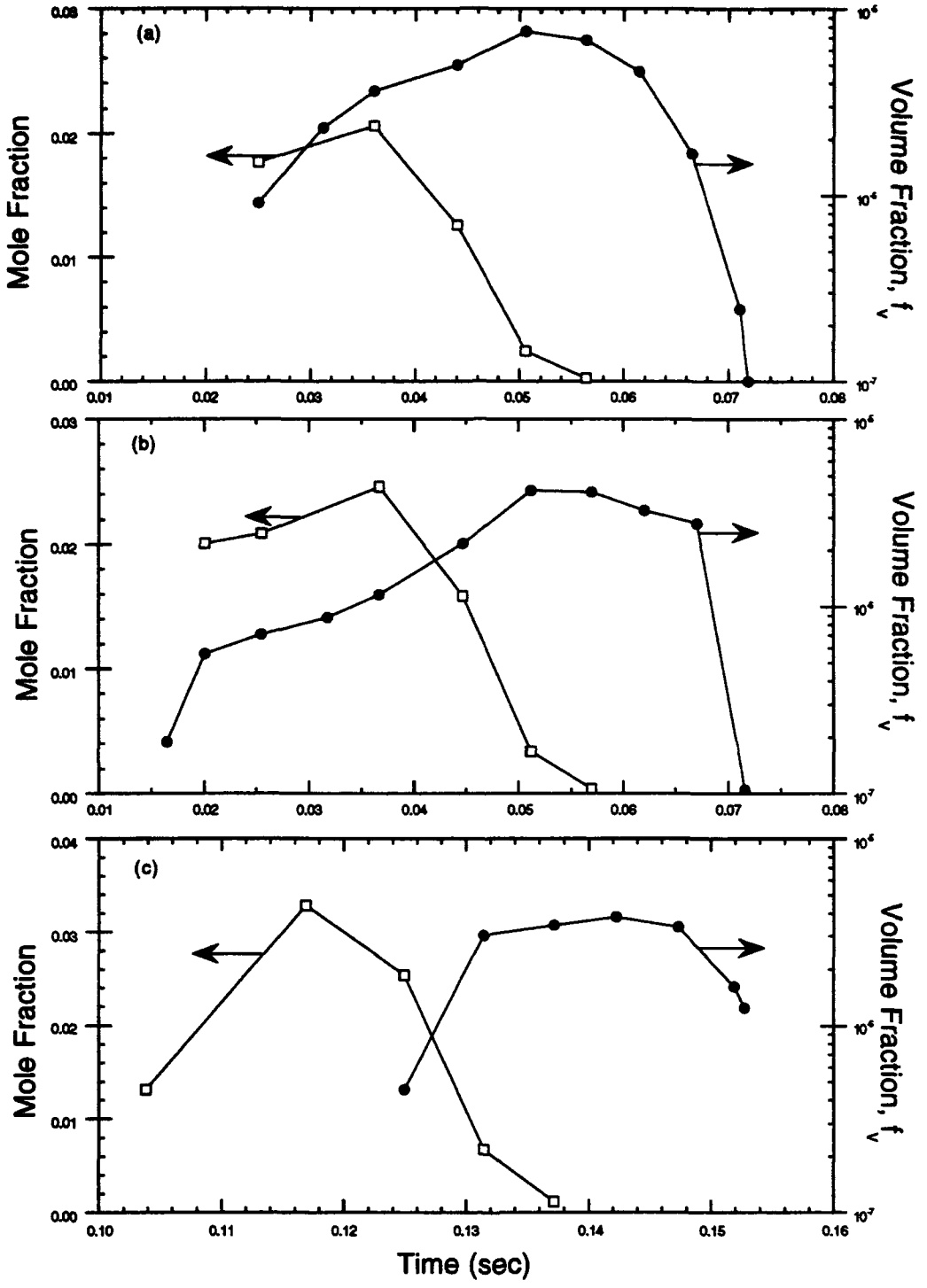

FIGURE 7 Plots of soot volume fraction, f_v, and the mole fraction of C_2H_2 as a function of time for a) the particle path containing the maximum f_v, b) the middle particle path , c) the particle path along the center line.

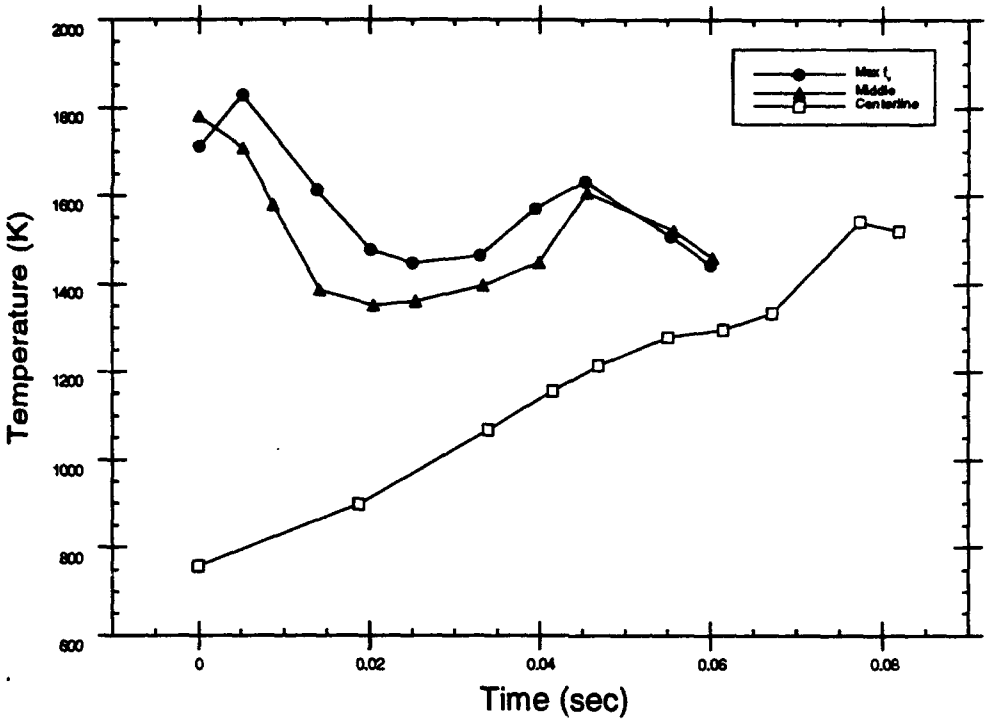

FIGURE 8 Calculated temperatures along particle paths as a function of time since the first detectable soot measurement.

Appendix B: Modeling and Measurements of Soot and Species in a Laminar Diffusion Flame

by

I. M. Kennedy, Darrell C. Rapp, R. J. Santoro and C. Yam

Submitted for presentation at the Twenty-fifth International Symposium on Combustion.

Modeling and Measurements of Soot and Species in a Laminar Diffusion Flame

Ian M. Kennedy*, Darrell C. Rapp#, Robert J. Santoro# and Clement Yam*

* Department of Mechanical and Aeronautical Engineering,
University of California,
Davis CA 95616
U.S.A.
and
Department of Mechanical Engineering,
The Pennsylvania State University,
University Park, PA 16802
U.S.A.

Corresponding author: Ian Kennedy
Department of Mechanical and Aeronautical Engineering
University of California,
Davis CA 95616
U.S.A.

Phone: (916) 752 2796
FAX: (916) 752 4158
Email: IMKENNEDY@UCDAVIS.EDU

Word Count:		
	Main text (by word processor count)	3533
	1 Table	200
	6 Figures	1200
	34 lines in nomenclature	238
	11 equations	231
	Total	5402

Subject Matter:		
	10.3	Soot, PAH
	3.5	Laminar Flames (Diffusion)
	4.0	Fires

Oral Presentation is preferred
Publication in Combustion and Flame is preferred
Code Letters: B and E

Abstract

A model of a laminar, ethene diffusion flame has been developed and compared with measurements. A system of elementary reactions is used to describe the gas phase C_1 and C_2 chemistry. The model incorporates a simple description of the growth of soot which performs a good job of reproducing the amount of soot in the flame and the transition from non-sooting to sooting conditions. Stable gas phase species have been measured in the flame with a combination of gas chromatography and mass spectrometry. Laser-induced fluorescence was used to measure the OH concentration. The model predicted most of the species quite well. It was found that the assumption of equilibrium concentrations for the minor radical species was grossly in error, particularly near the end of the flame where temperatures were low. Calculated radical species were found in concentrations that were orders of magnitude greater than equilibrium. Comparisons with measured OH concentrations supported this observation.

Introduction

Previous studies of a laminar ethene - air diffusion flame have suggested that the modeling of soot formation with the assumption of equilibrium chemistry may underestimate significantly the super-equilibrium concentrations of important radicals such as O and OH[1],[2]. These species are important oxidants of soot, particularly near the tip of diffusion flames where soot can escape. The original code that has been developed at U. C. Davis made use of the equilibrium assumption[2],[3] in order to determine the mole fractions of all the species in the flame. Finite rate chemistry is required in order to relax this assumption. An entirely new code was written to accommodate this modification. Detailed chemistry has been incorporated into a parabolic code that solves the boundary layer form of the conservation equations for mass, momentum and energy conservation. A much more accurate representation of radical concentrations has been achieved. Furthermore, interesting questions that are related to the interaction of soot with flame chemistry can now be investigated. The results of the modeling have been compared with the results of an experimental program at The Pennsylvania State University.

Experimental Method

A laminar ethene/air diffusion flame was established on a co-annular burner similar in design to that used in previous studies[4] and only a brief description will be given here. This burner consists of a 11.1 mm diameter brass fuel tube surrounded by a 102 mm diameter air annulus. A brass cylindrical chimney was used to shield the flame from laboratory air currents with access for sampling provided by slots machined in the chimney wall. The ethene (C2H4) and air flow rates were 3.85 $cm^3\ s^{-1}$ and 713 $cm^3\ s^{-1}$ respectively, which were measured with calibrated rotameters. Ethene with a stated purity of 99.5% was used; dried, filtered air was supplied by an in-house compressor.

Radial profile measurements of species concentrations have been obtained throughout the flame using an intrusive quartz microprobe sampling approach. Quartz microprobes have been used in many studies to perform the extraction of gas samples from premixed flames [5],[6] and diffusion flames[7], [8], [9], [10], [11]. Until recently their use has been limited to regions where the soot volume fraction is low to avoid clogging the probe orifice. A variation of the standard quartz microprobe design, referred to as an Electro-Mechanical Sonic (EMS) probe, was developed by Puri [11] and enabled sampling in flame regions where volume fractions were on the order of 10^{-5}. This probe has a fiber which extends through the orifice and is attached to a solenoid core with springs on either side of the core. A solenoid is placed around the outside of the quartz tube and the current to the solenoid is interrupted at about 30 Hz, providing for constant motion of the fiber in the orifice, thus keeping an annular region open for gas sampling. The fiber is ≈125 μm in diameter and is made from sapphire, while the orifice diameter is ≈190 μm. The annular sampling region has an area equivalent to a ≈130 μm diameter orifice.

A gas chromatograph and a mass spectrometer (MS) were used to analyze the samples. The use of these two techniques offered an independent verification of the concentration profile measurements as well as providing specific species measurement capability as described below. In general, the two analytical approaches yielded agreement to within ±20%. Because of difficulties in detecting H_2 with the GC, the MS measurements provide the determinations for this species. Since all of the data reported in this paper were obtained using the MS. only this instrumentation will be described in further detail.

The mass spectrometer employed an Extrel model 7-324-9 quadrupole mass filter with mass range of 1-500 amu for separation of ions and an electron multiplier for detection. Calibration of the MS employed a method used by Korobeinichev [12] which is mathematically similar to that of Bittner [13] and Crowhurst and Simmons[9]. The method relies on the signal response relative to other species remaining constant. That is, given the

same mixture, the signals of two gases will always be in the same ratio and is therefore independent of mass flow through the orifice due to any possible orifice clogging or variations in density. Secondly, this method assumes that the species measured constitute all of the gases present and they are normalized to a mole fraction of one.

A limitation of the MS in this flame is the coincidence of C_2H_4, N_2 and CO at mass 28. For C_2H_4, the fragment at mass 27 was used as an independent measurement. Calibration of C_2H_4 at both masses 27 and 28 was necessary so that the signal contribution of C_2H_4 at mass 28 could be subtracted from the mass 28 signal.

Hydroxyl radical (OH•) concentration measurements were obtained in a previous study [1]. The OH• measurements were obtained using the output from a Nd:YAG pumped dye laser which was frequency doubled to produce a UV beam. The fluorescence signal was collected at 90° with an intensified cooled CCD camera. The laser wavelength was tuned to either 278.83 nm or 283.55 nm, corresponding to $S_{12}(8)$ and $Q_1(8)$ lines of the $A^2\Sigma^+ \leftarrow X^2\Pi_i$ (1,0) band of OH•, respectively. Filters attenuated elastically scattered light from soot particles and transmitted the (0,0) and (1,1) emission bands of OH•. Excitation of the $S_{12}(8)$ line of OH• was used in regions of low soot particle concentration while the stronger $Q_1(8)$ line was utilized when soot concentrations were high (see Puri et al. [1]).

Numerical Model

The most general formulation of the governing equations consists of the compressible Navier-Stokes equations, an equation to describe the conservation of energy and species transport equations that are elliptic in nature. The computer time to solve these fully elliptic equations is large [14] . A number of assumptions are introduced in the present model that permit a significant saving in computer time without a serious impact on accuracy. The boundary layer forms of the governing equations are solved with zero pressure gradient. Hence, the equations can be solved with a marching method. It is expected that the boundary layer assumption will introduce the greatest errors in the vicinity of the nozzle

exit. The flame that has been investigated in this study is relatively long, of the order of 7 nozzle diameters. Therefore, it is expected that the errors will not be large in the region of most interest in relation to soot oxidation, radiation and their impact on gas phase chemistry.

The equations are solved in primitive variable form. Hence, the steady state continuity equation

$$\frac{\partial(\rho u)}{\partial x} + \frac{1}{r}\frac{\partial}{\partial r}(r\rho v) = 0 \qquad [1]$$

is solved along with the momentum equation

$$\rho u \frac{\partial u}{\partial x} + \rho v \frac{\partial u}{\partial r} = \frac{1}{r}\frac{\partial}{\partial r}\left(\mu r \frac{\partial u}{\partial r}\right) + \rho g \qquad [2]$$

The energy equation is written in terms of the temperature as

$$\rho C_P\left(u\frac{\partial T}{\partial x} + v\frac{\partial T}{\partial r}\right) = \frac{1}{r}\frac{\partial}{\partial r}\left(r\lambda\frac{\partial T}{\partial r}\right) + q^R - \frac{1}{r}\frac{\partial}{\partial r}\left(r\,\rho T \sum_{n=1}^{N} Y_n C_{P,n} V_n\right) - \sum_{n=1}^{N} M_n h_n \dot{w}_n \qquad [3]$$

in which the complete diffusion velocity of species n is V_n

$$V_n = v_n + v_n^T + V_n^{corr} \qquad [4]$$

The divergence of the radiative heat flux is represented by q^R. The normal diffusion velocity of species n is given by

$$v_n = -\frac{D_n}{Y_n}\frac{\partial Y_n}{\partial r} \qquad [5]$$

and the contribution of the thermal diffusion phenomenon to the total diffusion velocity is given by

$$v_n^T = \frac{D_n \kappa_n}{X_n} \frac{1}{T} \frac{\partial T}{\partial r} \qquad [6]$$

The thermal diffusion ratio, κ_n, was obtained from CHEMKIN [15]. A correction diffusion velocity, V_n^{corr}

$$V_n^{corr} = - \sum_1^N Y_n (v_n + v_n^T) \qquad [7]$$

ensures that net diffusive flux of all gaseous species is zero. An equation is solved for N-1 species mass fractions

$$\rho u \frac{\partial Y_n}{\partial x} + \rho v \frac{\partial Y_n}{\partial r} = - \frac{1}{r} \frac{\partial}{\partial r} \{r \rho Y_n V_n\} + M_n \dot{w}_n \qquad [8]$$

with the Nth species being N_2. Finally, an equation is solved for the soot mass fraction, Y_{soot}

$$\rho u \frac{\partial Y_{soot}}{\partial x} + \rho v \frac{\partial Y_{soot}}{\partial r} = - \frac{1}{r} \frac{\partial}{\partial r} \{r \rho V_T Y_{soot}\} + \rho S(Y_{soot}, T, f) \qquad [9]$$

In this equation, the thermophoretic velocity is found from the appropriate expression for a free molecular aerosol [16]

$$V_T = - 0.55 \frac{\upsilon}{T} \frac{\partial T}{\partial r} \qquad [10]$$

The source term in equation (9) includes the contributions of soot nucleation ($\dot{w}_{nucl}$), soot surface growth ($\dot{w}_g$) and soot oxidation ($\dot{w}_o$)

$$S(Y_{soot}, T, f) = \dot{w}_{nucl} + \dot{w}_g - \dot{w}_o \qquad [11]$$

An equation for soot particle number density is not included. Rather, an average number density is assumed. The justification for this assumption is discussed by Kennedy et al.[3]

The rates of reaction for the surface growth and soot oxidation terms are identical to those used by Kennedy et al.[3].

Method of Solution

Initial Conditions

Initial conditions for all the major species as well as the temperature profiles are required in order to start the calculation. These initial conditions are obtained by first starting the calculations with an equilibrium chemistry model with the Shvab-Zeldovich approximation [17] so that the mixture fraction can be used to describe the scalar field. This is achieved by generating a table of mass fractions of all species, density and temperature as functions of mixture fra[illegible]ns with the chemical equilibrium code STANJAN [18]. The momentum, continuity and [illegible]ture fraction equations are then solved simultaneously. Once the mixture fraction profile is known, all the other dependent variables can be obtained by using the table. Numerical trials have established that reasonable initial conditions for the finite rate chemistry calculation can be obtained by using the mixture fraction/equilibrium calculation up to 0.15 nozzle diameters.

Chemical Mechanism

A "skeletal" mechanism has been used to describe concisely the C_1 and the C_2 reactions for ethene oxidation. The methane mechanism of Smooke et al [19] has been found to be numerically efficient and it has been implemented in the current code with the rates for all the C_1 chemistry from Reference [19]. It contains a sufficient degree of detail to describe methane oxidation for the purposes of this project. The C_2 chemistry is described by a series of reactions that convert C_2H_4 to C_2H_3 and C_2H_2. The immediate source of the rates for the C_2 reactions is the paper by Frenklach et al. [20] ; primary sources of the rate data may be found in that reference. The entire reaction mechanism is shown in Table 1

and is composed of 62 reactions involving 24 species. The important oxidation steps by O, O_2 and OH are included. The CO oxidation steps and the H_2 - O_2 steps are also included.

Table 1

Chemical Reaction Mechanism in the form $k = A T^{\beta} e^{-E/RT}$ in units of moles, cubic centimetres, seconds, Kelvin and calories/mole.

	A	β	E
1. CH2+OH → CH2O+H	3.00E+13	0	0
2. CH2+O2 → CO+OH+H	3.10E+13	0	0
3. C2H+H2 → C2H2+H	1.10E+13	0	2866.0
4. C2H+O2 → HCCO+O	6.02E+11	0	0
5. HCCO+H → CH2+CO	1.50E+14	0	0
6. C2H2+O → CH2+CO	7.81E+03	2.8	502.0
7. C2H2+OH → HCCOH+H	5.06E+05	2.3	13496.0
8. CH2CO+H → HCCO+H2	3.00E+13	0	8599.0
9. CH2CO+OH → HCCO+H2O	1.00E+13	0	2627.0
10. C2H3+O → CH2CO+H	3.00E+13	0	0
11. C2H3+O2 → CH2O+HCO	4.00E+12	0	-239.0
12. C2H3+M → C2H2+H+M	2.00E+38	-7.2	50567.0
13. C2H4+OH → C2H3+H2O	3.00E+13	0	2986.0
14. C2H4+M → C2H2+H2+M	2.60E+17	0	79230.0
15. C2H4+H → C2H3+H2	3.16E+11	7	8002.0

16. C2H4+O → CH3+HCO	1.60E+08	1.4	525.0
17. CH4+M → CH3+H+M	1.00E+17	0	86000.0
18. CH4+O2 → CH3+HO2	7.90E+13	0	56000.0
19. CH4+H → CH3+H2	2.20E+04	3.0	8750.0
20. CH4+O → CH3+OH	1.60E+06	2.4	7400.0
21. CH4+OH → CH3+H2O	1.60E+06	2.1	2460.0
22. CH2O+OH → HCO+H2O	7.53E+12	0	167.0
23. CH2O+H → HCO+H2	3.31E+14	0	10500.0
24. CH2O+M → HCO+H+M	3.31E+16	0	81000.0
25. CH2O+O → HCO+OH	1.81E+13	0	3082.0
26. HCO+OH → CO+H2O	5.00E+12	0	0
27. HCO+M → H+CO+M	1.60E+14	0	14700.0
28. HCO+H → CO+H2	4.00E+13	0	0
29. HCO+O → OH+CO	1.00E+13	0	0
30. HCO+O2 → HO2+CO	3.00E+12	0	0
31. CO+O+M → CO2+M	3.20E+13	0	-4200.0
32. CO+OH → CO2+H	1.51E+07	1.3	-758.0
33. CO+O2 → CO2+O	1.60E+13	0	41000.0

34. CH3+O2 → CH3O+O	7.00E+12	0	25652.0
35. CH3O+M → CH2O+H+M	2.40E+13	0	28812.0
36. CH3O+H → CH2O+H2	2.00E+13	0	0
37. CH3O+OH → CH2O+H2O	1.00E+13	0	0
38. CH3O+O → CH2O+OH	1.00E+13	0	0
39. CH3O+O2 → CH2O+HO2	6.30E+10	0	600.0
40. CH3+O2 → CH2O+OH	5.20E+13	0	34574.0
41. CH3+O → CH2O+H	6.80E+13	0	0
42. CH3+OH → CH2O+H2	7.50E+12	0	0
43. HO2+CO → CO2+OH	5.80E+13	0	22934.0
44. H2+O2 → 2OH	1.70E+13	0	47780.0
45. OH+H2 → H2O+H	1.17E+09	1.3	626.0
46. H+O2 → OH+O	2.20E+14	0	16800.0
47. O+H2 → OH+H	1.80E+10	1.0	8826.0
48. H+O2+M → HO2+M	2.10E+18	-1.0	0
49. H+O2+O2 → HO2+O2	6.70E+19	-1.4	0
50. H+O2+N2 → HO2+N2	6.70E+19	-1.4	0
51. OH+HO2 → H2O+O2	5.00E+13	0	1000.0

52. H+HO2 → 2OH	2.50E+14	0	1900.0
53. O+HO2 → O2+OH	4.80E+13	0	1000.0
54. 2OH → O+H2O	6.00E+08	1.3	0
55. H2+M → H+H+M	2.23E+12	.5	92600.0
56. O2+M → O+O+M	1.85E+11	.5	95560.0
57. H+OH+M → H2O+M	7.50E+23	-2.6	0
58. H+HO2 → H2+O2	2.50E+13	0	700.0
59. HO2+HO2 → H2O2+O2	2.00E+12	0	0
60. H2O2+M → OH+OH+M	1.30E+17	0	45500.0
61. H2O2+H → HO2+H2	1.60E+12	0	3800.0
62. H2O2+OH → H2O+HO2	1.00E+13	0	1800.0

Numerical Scheme

The governing differential equations are written in a discrete form by using a second order accurate scheme for the diffusion terms and first order accurate scheme for the convective terms with the delta formulation. The non-linear terms (convective and rate terms) are linearized by using Newton's method. The resulting Jacobian matrices are determined numerically in the manner described by Smooke [21] . The Jacobian does not need to be updated continuously since the changes from one step to the next step are small. We found

that the evaluation of the Jacobian at every fifth spatial step yielded the same results as an evaluation at every step.

The resulting sets of coupled algebraic equations are solved implicitly and simultaneously by the usage of a block solver with iterations to account for the non-linear term. Typically, 8 iterations per step are required to converge the equations to a local solution. The step size (Δx) is determined by limiting the maximum changes of all the dependent variables by no more than 10 percent. If the maximum changes in any dependent variable exceed this limit, the solution is rejected and a smaller Δx is used and the calculation is redone. The equations are assumed to be solved when the residual approaches machine zero. If a local convergence cannot be reached, a smaller Δx is used and the solution is recalculated.

Grid adaptation is used in order to resolve the high gradient region in the flow field with a minimum number of grid points. This is done by adapting the grid distribution to the temperature gradient. The results shown in this report are obtained by using only 61 points in the transverse direction. All the properties of the fluid, the diffusion coefficients of all species and the chemical source term for each species were obtained by using CHEMKIN [15] .

Results

Solutions for a non-sooting and a sooting flame are presented. The predicted integrated soot volume fractions are shown in Fig. 1; they are a measure of the total amount of soot at a given axial plane. Experimental data from Santoro et al. [22] are also shown in Figure 1 . The agreement between the model predictions and the measurements of the integrated soot volume fraction is considered quite good. Burn out of soot at the end of the flame is evident. Generally, the soot model tends to underpredict the measured values of soot volume fraction. However, the spatial distribution of soot is reproduced very well including the location of the peak integrated soot volume fraction. Although it is not shown in this paper, the model manages to reproduce the transition from a non-sooting flame to a

sooting flame quite well as the fuel flow rate is increased. The agreement that is shown in Fig. 1 , along with more detailed radial profiles of soot volume fractions which are not shown, provide the basis for confidence in the application of this relatively simple soot model to a calculation of detailed chemistry in an ethene flame.

In addition to a simple soot model, the code includes a radiation model, in which an optically thin model is adopted for simplicity. A comparison of the measured and predicted temperature fields offers a measure of its accuracy. Figure 2 presents radial profiles of the measured and predicted temperatures at two axial locations in the non-sooting flame. The drop in the peak temperature at the more downstream location is evidence of the heat loss due to luminosity. The agreement in the temperature field is considered good, although the radiation model leads to underprediction of the radiative heat loss, in part because gas radiation is ignored and also because the soot volume fractions are underpredicted. Similar agreement is evident in the velocity field although these results are not shown.

The fuel mole fractions in the non-sooting flame are shown in Fig. 3 at a location that is 7 mm from the fuel nozzle. A profile of C_2H_2 mole fractions at the same location is shown in Fig. 4 . There is a general tendency to overpredict the measured mole fractions of C_2H_4 and C_2H_2 in the central region of the flame while the model results show steeper gradients as the radial location increases. The finite spatial resolution of the EMS probe contributes to the observed differences in this region since species concentration gradients in the flame are steep. Further improvement in the comparisons between model and experiments will require higher spatially resolved measurements and consequently the current agreement is considered satisfactory for model validation. The loss of C_2H_2 onto soot is not accounted for at present in the balance equation for acetylene. This sink of acetylene could reduce the predicted C_2H_2 concentrations, particularly further downstream where soot mass growth rates are more intense. The hydrogen mole fraction profile at 7 mm is shown in Fig. 5 . The calculated values exhibit reasonably good agreement with the experimental data in view

of the difficulty in measuring this species. At a location 20 mm from the fuel nozzle, the H_2 distribution has moved towards the centerline as the flame reaction zone approaches the centerline. The results indicate that the general structure of this luminous flame is reproduced quite well by the numerical model.

Hydroxyl mole fractions have been measured with laser induced fluorescence. The calculated hydroxyl mole fractions are compared with the measurements at 7 mm and 70 mm in Fig. 6 . The model tends to overpredict the OH mole fractions. This tendency may be due, in part, to the absence of a numerical sink for OH on soot particles. The model does not incorporate this aspect of the physics at present. A full coupling of the flame chemistry and the soot chemistry will be attempted in the future with a modified soot model that will incorporate elementary steps for soot mass growth and oxidation. It must also be born in mind that LIF measurements involve uncertainties that are related to quenching corrections and other errors. The errors were estimated to be ±50% [1].

The preceding comparison of numerical and experimental results provides grounds for some confidence in the results of the calculations. The use of a detailed kinetics model with a model for soot formation and radiation permits us to examine questions regarding the impact of the soot process on flame chemistry in a manner that experiments alone cannot attempt. For example, calculations of turbulent flames require a model for the thermochemistry. A convenient and very common approach is to use chemical equilibrium. It is instructive to examine the accuracy of this assumption when there is substantial radiative heat loss from a hydrocarbon flame. The non-equilibrium effect is greatest for the minor, radical species such as O and OH. These species are of particular interest in the formation and oxidation of pollutants such as NO and soot. The ratio of computed OH mole fractions to equilibrium mole fractions at the local computed temperature were calculated at 40 mm from the nozzle . At a radius of r/D = 0.745, $\frac{OH_{numerical}}{OH_{eq}} = 22$ while

$\frac{O_{numerical}}{O_{eq}} = 478$. This location is to the air side of the reaction zone at a mixture fraction of around 0.03 (stoichiometric mixture fraction is 0.064). It is apparent that large super-equilibrium concentrations can be achieved as a result of the depressed temperatures in this radiating flame. Puri et al. [1] found that the OH super-equilibrium ratio was 9.4 at the peak OH location in this flame at a height of 70 mm. The results suggest that assumption of equilibrium chemistry is grossly inadequate for the prediction of the minor species.

Conclusions

The interaction of soot and the flame chemistry has been modeled with a relatively simple fluid and chemical scheme. A comparison of the numerical results with detailed experimental results indicates that the flame structure is reproduced quite well. Radicals such as OH and O are predicted to be present in concentrations that are significantly greater than equilibrium. The degree of super-equilibrium is a function of the temperature and, hence, the soot loading in the flame. Future work requires the addition of sink terms in the species equations for OH and C_2H_2. It should be possible to treat other fuels by including a small number of additional reactions for the pyrolysis of the parent fuel to C_2 species.

Acknowledgments

The group at Davis acknowledge gratefully the support of the National Institute of Standards and Technology through Grant 60NANBOD1055, NSF through Grant CTS-8857477 and the National Institute of Environmental Health Sciences Superfund Basic Research Program 2 P42 ES04699.

The research at The Pennsylvania State University was supported under grant F49620-92-J-0161 from the Air Force Office of Scientific Research (AFOSR) and grant 60NANBOD1035 from the National Institute of Standards and Technology. One of the authors (DCR) would like to thank the support of the Air Force Research in Aero Propulsion Technology Program sponsored by the AFOSR during his tenure.

Nomenclature

A	pre-exponential factor in rate coefficient
C_P	specific heat at constant pressure
D	nozzle diameter
D_n	effective diffusivity of species *n* in the mixture
E	activation energy
f	mixture fraction
g	gravitational acceleration
h_n	specific enthalpy of species *n*
k	rate coefficient
M_n	molecular weight of species *n*
N	number of species
q^R	divergence of the radiative heat flux vector
R	gas constant
r	radial distance
S	source or sink term for soot equation
T	temperature
u	velocity in the axial direction

v velocity in the radial direction

v_n normal diffusion velocity of species *n*

v_n^T thermal diffusion velocity of species *n*

V_n^{corr} correction to diffusion velocities

V_T thermophoretic velocity of soot particles

$\dot{w}_n$ reaction rate of species *n*

X_n mole fraction of species *n*

x distance along the axis

Y_n mass fraction of species *n*

β exponent on temperature in rate coefficient

κ_n thermal diffusion ratio

λ thermal conductivity

μ absolute viscosity

ν kinematic viscosity

ρ density

Subscripts

eq equilibrium

g soot mass growth

n soot nucleation

numerical calculated with computer code

o soot oxidation

References

[1] PURI, R., MOSER, M., SANTORO, R. J. and SMYTH, K. C., *Twenty-Fourth Symposium (International) on Combustion*,, The Combustion Institute, Pittsburgh,1992, pp. 1015-1022.

[2] VILLASENOR, R. and KENNEDY, I. M., *Twenty-Fourth Symposium (International) on Combustion*, The Combustion Institute, Pittsburgh, 1992., pp. 1023 - 1030.

[3] KENNEDY, I. M., KOLLMANN, W. and CHEN, J.-Y., *Combust. Flame* 81: 73 - 85 (1990).

[4] SANTORO, R. J., SEMERJIAN, H. G. and DOBBINS, R. A., *Combust. Flame* 51: 203-218 (1983).

[5] FRISTROM, R. M.,PRESCOTT, R., GRUNFELDER, C., *Combust. Flame* 1: 102-113 (1957).

[6] BOCKHORN, H., FETTING, F., WENZ, H. W., *Berichte der Bunsen-Gesellschaft für Physikalische Chemie* 87: 1067-1073 (1983).

[7] SMITH, S. R. and GORDON, A. S., *J. Phys. Chem.* 60: 759-763 (1956).

[8] MITCHELL, R. E., *Nitrogen oxide formation in laminar methane-air diffusion flames*, Ph. D. Thesis, Massachusetts Institute of Technology (1975).

[9] CROWHURST, D. and SIMMONS, R. F., *Combust. Flame* 59: 167-176 (1985).

[10] SMYTH, K. C., MILLER, J. H.. DORFMAN, R. C., MALLARD, W. G., SANTORO, R. J., *Combust. Flame* 62, 157-181 (1985).

[11] PURI, R., *The Interaction of Soot Particles with Carbon Monoxide in Laminar Diffusion Flames*, Ph. D. Thesis, The Pennsylvania State University (1992).

[12] KOROBINECHEV, Combus. Expl. Shock Waves 23(5): 565-576 (1987).

[13] BITTNER, J. D., *A Molecular Beam Mass Spectrometer Study of Fuel-Rich and Sooting Benzene-Oxygen Flames*, Ph. D. Thesis, Massachusetts Institute of Technology (1981).

[14] SMOOKE, M. D., XU, Y., ZURN, R. M., LIN, P., FRANK, J. H. and LONG, M. B., *Twenty-Fourth Symposium (International) on Combustion,* The Combustion Institute, Pittsburgh, 1992,pp. 813 - 821.

[15] KEE, R. J., RUPLEY, F. M. and MILLER, J. A., *The Chemkin Thermodynamic Data Base*, Sandia National Laboratories, Livermore (1992).

[16] TALBOT, L., CHENG, R. K., SCHEFER, R. W. and WILLIS, D. R., *J. Fluid Mech.* 101: 737 - 758 (1980).

[17] WILLIAMS, F. A., *Combustion Theory*, The Benjamin/Cummings Publishing Co. 1985.

[18] REYNOLDS, W. C., *STANJAN*, Department of Mechanical Engineering, Stanford University, Stanford CA, 1986.

[19] SMOOKE, M. D., PURI, I. K. and SESHADRI, K., *Twenty-First Symposium (International) on Combustion*,, The Combustion Institute, Pittsburgh, 1986, pp. 1783 - 1792.

[20] FRENKLACH, M., WANG, H. and RABINOWITZ, M. J., *Prog. Energy Combust. Sci.* 18: 47 - 73 (1992).

[21] SMOOKE, M. D. and GIOVANGIGLI, V., *Impact of Computing in Science and Engineering* 4: 46 - 79 (1992).

[22] SANTORO, R. J., YEH, T. T., HORVATH, J. J. and SEMERJIAN, H. G., *Combust. Sci. Tech.* 53: 89-115 (1987).

Figure Captions

Fig. 1 Measured and predicted soot volume fractions integrated across a non-sooting flame

-------- calculations

■ experiments

Fig. 2 Measured and predicted temperature profiles

-------- calculations

■ experiments at 7 mm from nozzle exit

▲ experiments at 70 mm from nozzle exit

Fig 3 Measured and predicted C_2H_4 mole fractions at 7 mm from the nozzle

-------- calculations

■ experiments

Fig. 4 Measured and predicted C_2H_2 mole fractions at 7 mm from the nozzle

-------- calculations

■ experiments

Fig. 5 Measured and predicted H_2 mole fractions at 7 mm from the nozzle

-------- calculations

■ experiments

Fig. 6 Measured and predicted OH mole fractions

-------- calculations

■ experiments at 7 mm from nozzle exit

▲ experiments at 70 mm from nozzle exit

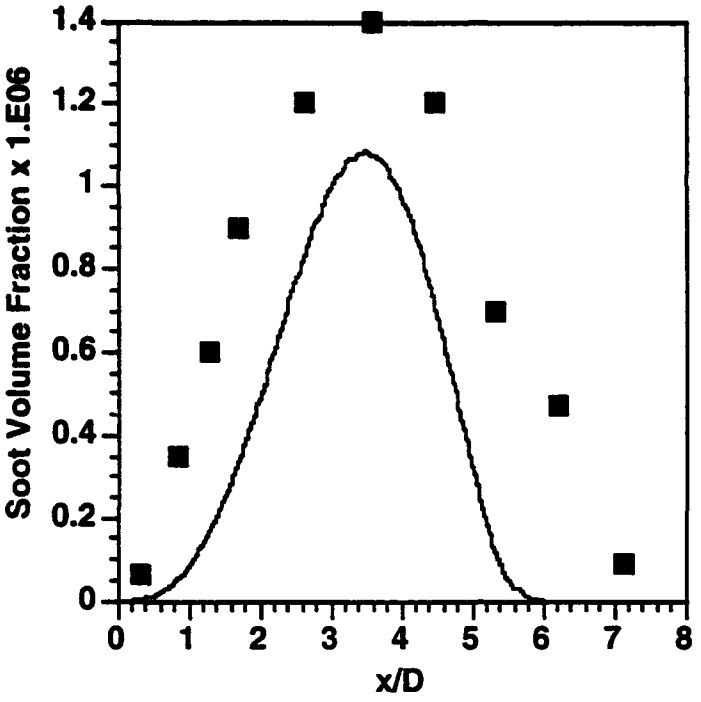

fig 1

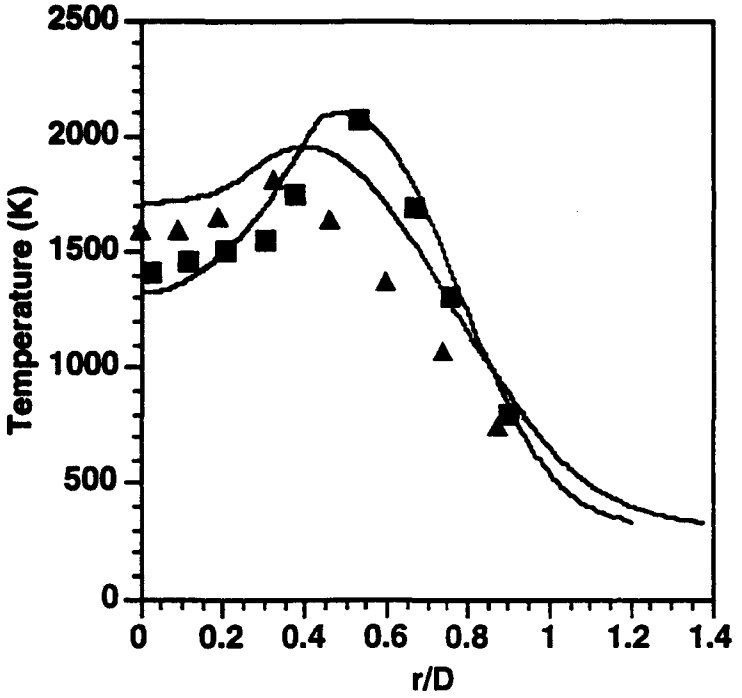

fig 2

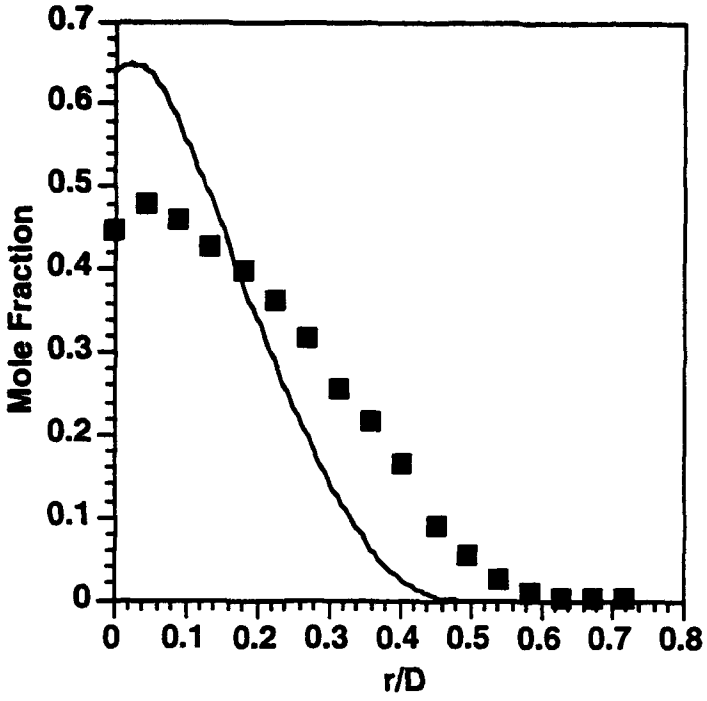

fig 3

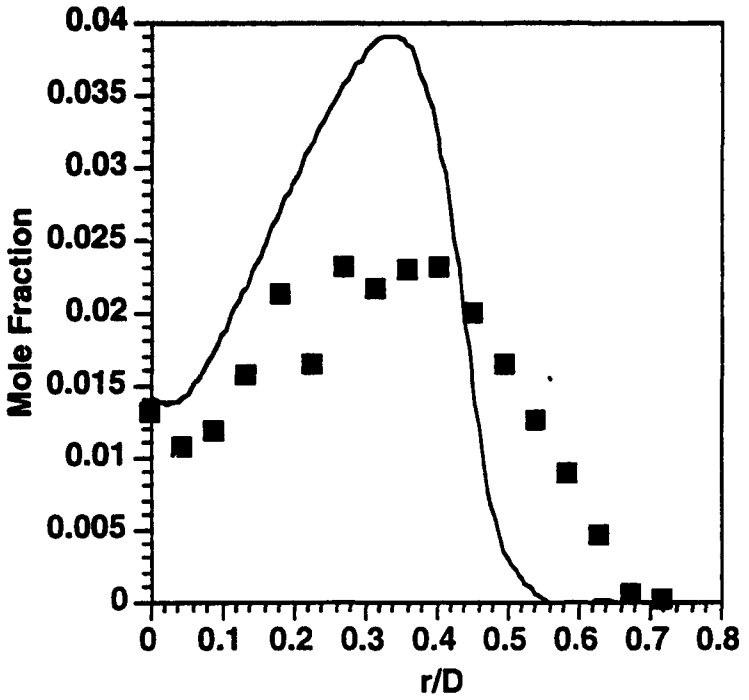
0.04
0.035
0.03
0.025
0.02
0.015
0.01
0.005
0
Mole Fraction
0
0.1
0.2
0.3
0.4
0.5
0.6
0.7
0.8
r/D

fig 4

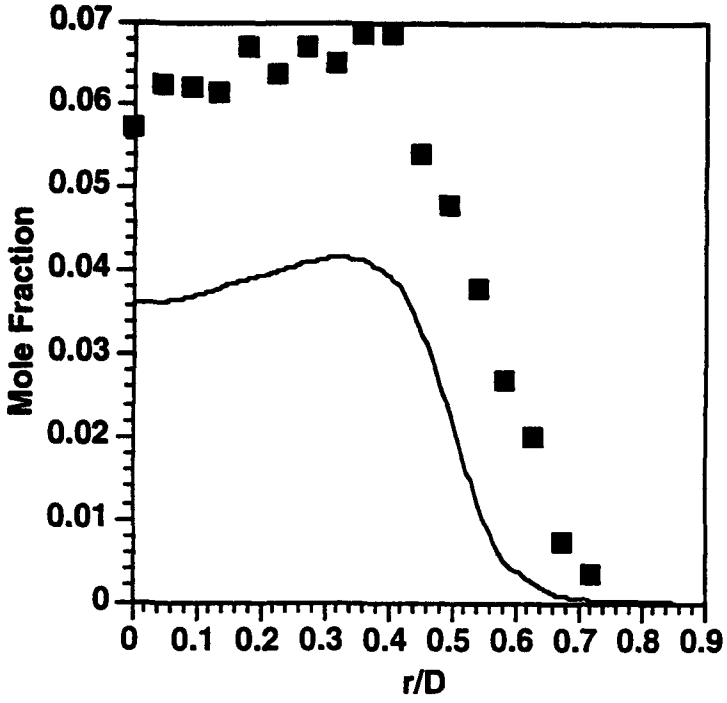
0.07
0.06
0.05
0.04
0.03
0.02
0.01
0
Mole Fraction
0 0.1 0.2 0.3 0.4 0.5 0.6 0.7 0.8 0.9
r/D

fig 5

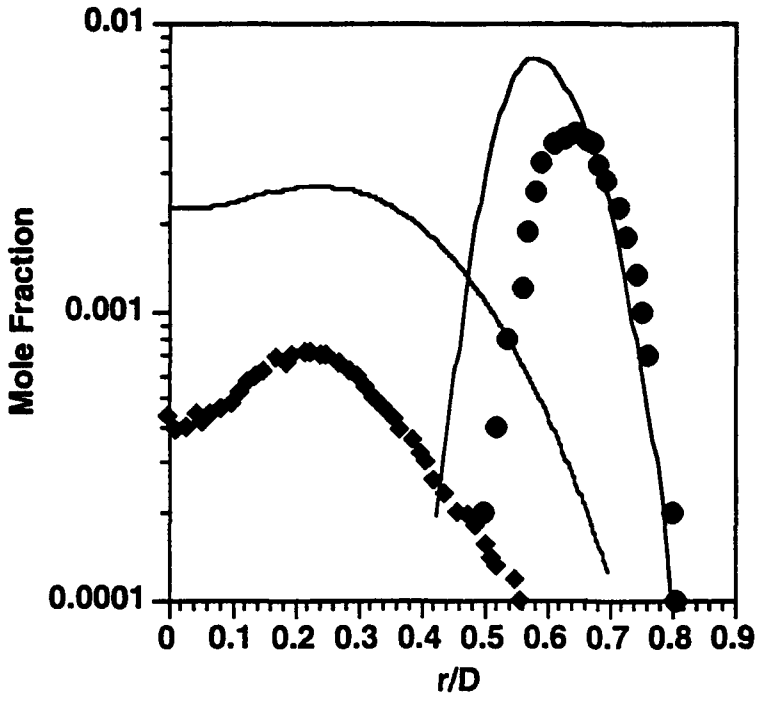

fig 6

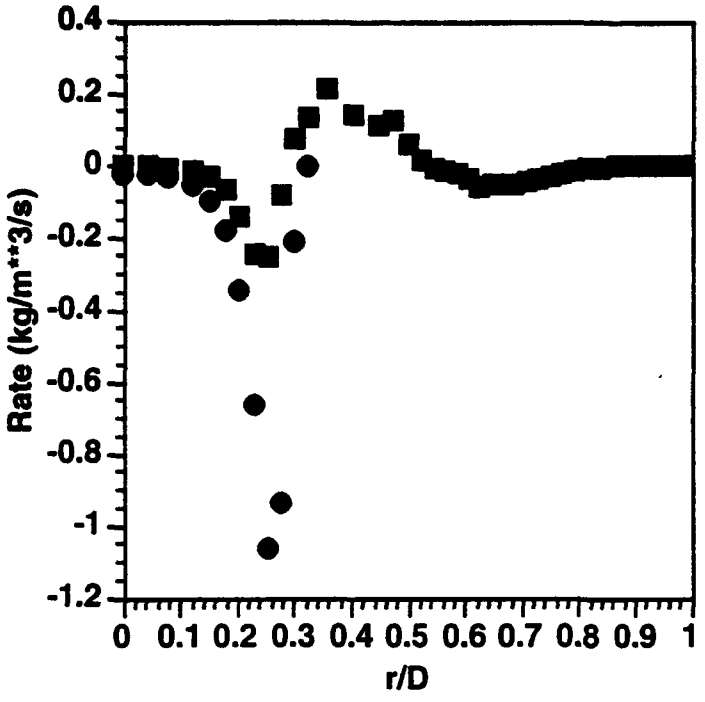

fig 7

Appendix C: Spatially-Resolved Measurements of Soot Volume Fraction Using Laser-Induced Incandescence

by

B. Quay, T-W Lee, T. Ni and R. J. Santoro

Combustion and Flame (in press)

SPATIALLY-RESOLVED MEASUREMENTS OF SOOT VOLUME FRACTION USING LASER-INDUCED INCANDESCENCE

B. Quay, T.-W. Lee, T. Ni and R. J. Santoro
Department of Mechanical Engineering
The Pennsylvania State University
University Park, PA 16802

Abstract- Laser-induced incandescence is used to obtain spatially-resolved measurements of soot volume fraction in a laminar diffusion flame, in which comparisons with laser scattering/extinction data yield excellent agreement. In addition, the laser-induced incandescence signal is observed to involve a rapid rise in intensity followed by a relatively long (ca. 600 ns) decay period subsequent to the laser pulse, while the effect of laser fluence is manifest in non-linear and near-saturated response of the laser-induced incandescence signal with the transition occurring at a laser fluence of approximately 1.2×10^8 W/cm^2. Spectral response of the laser-induced incandescence involves a continuous spectrum in the visible wavelength range due to the blackbody nature of the emission. Simultaneous measurements of laser-induced incandescence and light-scattering yield encouraging results concerning the mean soot particle diameter and number concentration. Thus, laser-induced incandescence can be used as an instantaneous, spatially-resolved diagnostic of soot volume fraction without the need for the conventional line-of-sight laser extinction method, while potential applications in two-dimensional imaging and simultaneous measurements of laser-induced incandescence and light-scattering to generate a complete soot property characterization are significant.

INTRODUCTION

Formation, growth and oxidation of soot particles in diffusion flames involve a complex interaction between chemistry and fluid mechanics. The understanding of these chemical and physical processes is important not only from a fundamental scientific standpoint, but also due to their applications in practical combustion devices. For example, soot emission from automotive and gas turbine engines constitutes one of the major pollutants that needs to be minimized, while excessive soot formation and radiation in propulsion devices have adverse effects on combustor and flow components. In this regard, sooting characteristics of both turbulent and laminar flames have been investigated by numerous researchers, while in this laboratory attention has been focused on axisymmetric laminar diffusion flames. The soot property measurements made in this flame, thus far, involve the laser scattering/extinction method. This technique yields measurements of soot volume fraction, mean soot particle diameter, and number density after tomographic inversion of the laser extinction data due to the line-of-sight nature of these measurements.

However, recent studies of a process involving laser-induced incandescence (LII), in which the soot particles are heated up by the laser energy and emit blackbody radiation or incandescence at elevated temperatures, have shown that LII can be used as a non-intrusive spatially-resolved soot diagnostic [1-6]. In particular, it has been pointed out by Melton [1] that the LII signal is nearly proportional to the local soot volume fraction for sufficiently large laser [illegible]; thus, a pointwise measurement of soot volume fraction can be made without the need for the line-of-sight laser extinction and time-consuming tomographic inversion method. While other applications of LII in soot diagnostics, for measurements of soot particle size distribution for example, have been suggested [1], the most direct and significant application of LII may be in obtaining point measurements of soot volume fraction since the line-integral nature of laser extinction and subsequent tomographic inversion technique have deficiencies in some laminar flame and most turbulent flame configurations. For example, instantaneous measurements of local soot volume fraction can be made in turbulent diffusion

flames using LII without being limited to time-averaged data or an axisymmetric burner geometry. Furthermore, applications of LII in investigations of soot properties include two-dimensional imaging of soot volume fraction distributions and simultaneous LII and light-scattering measurements to construct a complete soot property characterization. Recently, qualitative information on soot formation under Diesel engine conditions has been reported in which simultaneous two-dimensional LII and light-scattering images were obtained [5,6].

In spite of these potentially significant applications of LII in soot diagnostics, no experimental verification of the LII technique for determining the local soot volume fraction has been reported to date. The objectives of this investigation, therefore, were to experimentally determine the applicability of the LII method to obtain spatially-resolved measurements of soot volume fraction, to study the feasibility of making simultaneous LII and light-scattering measurements to obtain a complete soot property characterization, as well as to investigate the detailed characteristics of LII in laminar diffusion flames.

LASER-INDUCED INCANDESCENCE

Laser-induced incandescence involves the heating of soot particles to temperatures above the surrounding gas temperature due to the absorption of laser energy, and subsequent detection of the blackbody radiation corresponding to the elevated soot particle temperature. The temperature of the soot particle is determined by the rate of laser energy absorption, conductive heat transfer to the surrounding gas, soot vaporization, and radiative heat loss through blackbody radiation [1,2]. For example, a Nd:YAG pulsed laser beam of ca. 7 ns duration used in the present laser-induced incandescence measurements represents an energy source in the energy balance equation, and the soot particle temperature rapidly rises during the duration of the laser pulse as the soot particles absorb the laser energy. The heat sink terms in this phase are the conductive and radiative heat losses to the surrounding gas, which are much smaller than the laser energy absorption rate for laser fluence levels relevant to laser-induced incandescence. Near a soot particle temperature of ca. 4000 K, which is

close to the soot vaporization point, the temperature rise is severely curtailed by the energy expended in the vaporization of soot particles [1], although soot surface temperatures as high as 5000 K have been observed for sufficiently large laser fluence [7]. Subsequent to the laser pulse, the temperature of the soot particles gradually decreases due to conductive and radiative heat losses.

The intensity of the laser-induced incandescence, or the blackbody radiation due to laser heating, for a single soot particle has a dependence on the soot particle temperature, detection wavelength, and the laser fluence. The total incandescence emitted from the soot particle surface has a fourth-order dependence on the soot particle temperature. The spectral shape of the incandescence is determined by Planck's law with the maximum in the blackbody radiation occurring at a wavelength inversely proportional to the soot particle temperature according to Wien's displacement law. Thus, the temporal variation in the laser-induced incandescence signal at a given detection wavelength qualitatively follows the soot particle temperature in time, with the exact functional relationship determined by the processes described above.

Computations of the laser-induced incandescence in response to an idealized laser pulse based on the above blackbody radiation laws and the soot particle energy balance have been performed by Melton [1] and Tait and Greenhalgh [4]. In particular, in the limit of high laser power and maximum soot particle temperature near its vaporization point, Melton [1] has shown that the intensity of the laser-induced incandescence signal for a group of soot particles has a dependence on mean soot particle diameter raised to the power of $(3 + 0.154\lambda_{det}^{-1})$, where λ_{det} is the detection wavelength expressed in microns. For λ_{det} between 0.7 and 0.4 μm, for example, the laser-induced incandescence signal is proportional to the mean soot diameter raised to the power of 3.22 to 3.38, or approximately to the soot volume fraction. This forms the basis for the current approach of using laser-induced incandescence for pointwise measurement of soot volume fraction.

EXPERIMENTAL METHODS

The experimental apparatus involved a coannular laminar diffusion flame burner which was identical to the burner employed in this laboratory in previous studies of soot properties [8-10]; thus, only a brief description will be given here. The overventilated laminar flame burner consisted of two concentric brass tubes with fuel and air flowing through the inner (11.1 mm ID) and outer (101.6 mm ID) tubes, respectively, where the fuel tube extended 4 mm beyond the exit plane of the air tube. Flow conditioning for the air was achieved via a layer of 3.0 mm glass beads, a series of wire screens and a ceramic honeycomb section, while the fuel passage contained a layer of 3.0 mm glass beads and a single wire screen. A 405 mm long brass cylinder that fit over the outer tube was used as a chimney to shield the flame from laboratory air disturbances; and optical access was obtained through machined slots on the brass cylinder which traversed with the burner assembly. In addition, screens and a flow restrictor were placed at the chimney exit to achieve a highly stable flame similar to previous studies [8-10]. The traverse system involved a stepper motor and controller (Daedal PC-410-288) which provided positioning capability with a resolution of 0.0127 mm.

The optical setup for the laser-induced incandescence included an Nd:YAG pulse laser (Continuum Model NY61-10), the output beam of which was ca. 7 ns in duration and was focused to approximately 0.38 mm in diameter using a bi-convex lens of 400 mm focal length. The probe volume location was displaced ~ 25 mm from the focal point of the lens in order to achieve this 0.38 mm diameter. A schematic of the optical arrangement is shown in Fig. 1. Both the 1064 nm and frequency-doubled 532 nm beams from the Nd:YAG laser were used, the diameter of which prior to the focusing lens was approximately 9 mm with a nearly Gaussian profile. In order to observe the effect of varying the laser fluence for the 532 nm wavelength, a combination of a half-wave plate, mounted in a rotation stage, in series with a polarizing beam splitter was used to attenuate the laser energy by a varying amount. A neutral density filter (0.7 N.D.) preceded the half-wave plate to reduce the laser power to an acceptable value. By rotating the half-wave plate to vary the ratio of

vertically polarized to horizontally polarized light, in conjunction with aligning the beam splitter to transmit only the vertically polarized portion of the beam, laser energies ranging from 0.2 to 3.3 mJ were obtained corresponding to laser fluence between 2.5×10^7 and 4.2×10^8 W/cm^2. The laser energy was monitored during the experiment using a pyrometer (Molectron J1000), and was maintained during the actual measurements of the soot volume fraction at 2.4 mJ for a laser fluence of 3.0×10^8 W/cm^2 in order to minimize the effect of laser beam attenuation across the flame (see discussion below). The laser-induced incandescence signal was collected at a 90° angle using a focusing lens with an f-number of 3 at unit magnification. Except for the spectral scans, an interference filter (400 ± 10nm) was placed in front of the monochromator to minimize interference from light scattering. For the spectral scans, the interference filter was removed from in front of the monochromator and the 1064 nm wavelength laser probe beam was used to produce the LII signals. For these measurements, a series of neutral density filters were used to vary the laser fluence rather than the half-wave plate/beam splitter arrangement used with the 532 nm wavelength laser probe beam.

Since the LII signal had a continuous spectrum in the visible wavelength range, while interference from light-scattering and PAH fluorescence was expected near wavelengths of 532 nm and above [10,11], the detection of the LII signal was made at a wavelength of 400 nm for both 532 nm and 1064 nm wavelength probe laser beams. Measurements made at 500 and 700 nm detection wavelengths for the 1064 nm wavelength probe laser yielded identical results due to the continuous nature of the LII spectrum in the visible wavelength range. The detection wavelength was set by using a 0.25m-monochromator (Instruments SA H20) with a grating blazed at 330 nm with 1 mm x 1 mm slits, which also defined the length of the probe volume. The bandpass of the monochromator was estimated to be 4 nm FWHM, while the spectral response of the monochromator was calibrated using an incandescent lamp (Eppley T24). A photomultiplier tube (Hammamatsu R928) was connected to the exit slit of the monochromator, the signal from which was conditioned using a

boxcar integrator with a gate width of 10 ns and averaged over 100 laser shots.

Temporal variations of the LII signal were observable by moving the boxcar gate in 2-10 ns increments. LII profiles across the flame and spectral characteristics of the LII signal were observed by using the burner traverse system described above and by the scanning of the detection wavelength via the monochromator, respectively. The measurements were made in non-smoking ethylene/air diffusion flames where the ethylene and air flow rates were 3.85 cm^3/s and 1060 cm^3/s, respectively.

RESULTS AND DISCUSSION

Figure 2 shows a typical temporal variation of the LII and vertically-polarized light-scattering signals taken at a height of 40 mm above the fuel tube exit for an ethylene laminar diffusion flame at the radial location where the peak soot volume fraction is observed (r=2.5 mm). The variation of the LII signal in time has been obtained by increasing the boxcar gate delay in 2-10 ns increments with respect to the laser pulse while averaging over 100 laser shots, as described above. It can be observed in Fig. 2 that the initial phase of the signal involves a rapid rise in the LII signal intensity due to the increase in the soot particle temperature during the laser pulse of ca. 7 ns in duration. Subsequent to the peak in the LII signal, the soot particles undergo conductive and radiative heat loss to the ambient gas and the LII signal gradually decreases, although a sensible LII signal is still observed at approximately 600 ns after the laser pulse. The temporal variation of the LII signal shown in Fig. 2 is qualitatively very similar to the LII response function for an idealized laser pulse computed by Melton [1]. A characteristic time constant for the LII process for soot particles has been shown to be linearly proportional to the soot particle diameter [3], and is estimated to be approximately 700 ns for a diameter of 100 nm. The decay time observed in Fig. 2 is approximately 600 ns for the signal to decrease to 5% of the peak value, while the mean soot particle diameter (D_{63}) at this location is approximately 135 nm (see Fig. 7(b)). Thus, in contrast to the light-scattering signal, which is observable in principle only during the duration of the laser pulse due to its elastic scattering nature, the LII signal exhibits a much longer temporal characteristic as shown in Fig. 2.

Melton [1] has discussed the potential for obtaining particle size distribution parameters from the temporal behavior of the LII signal. Such information is better obtained using a shorter probe laser wavelength than that used in the present study and may also suffer from interference from laser-induced fluorescence from PAH species [1].

A comparison between the soot volume fraction measured by LII and the laser scattering/extinction technique is shown in Figs. 3 (a)-(c), where the soot volume fraction is plotted as a function of radial location at selected heights ranging from 10 to 70 mm above the fuel tube exit. The open and dark symbols represent laser scattering/extinction and LII data, respectively. The laser scattering/extinction data for soot volume fraction in this flame has been taken from Santoro et al. [8,9], and involves the well-known method of measuring the line-of-sight extinction of the laser beam followed by a tomographic inversion in order to reconstruct the local soot volume fraction. Further details of this technique and the data can be found in Santoro et al. [8,9]. In order to calibrate the observed LII signal, the LII signal at a single spatial point corresponding to the radial location where the peak soot volume fraction occurs (r=2.5 mm) at the 40 mm height has been equated with the known value of soot volume fraction at this location from the laser scattering/extinction measurements. All other LII data can then be converted to absolute soot volume fraction based on this single-point calibration procedure.

The radial profiles of soot volume fraction obtained in this manner, as shown in Figs. 3(a)-(c), exhibit the familiar physics of soot growth and oxidation in this flame. At low heights, soot particles are observed in the annular region on the fuel-rich side of the flame. Soot formed in this region undergoes net growth with increasing height up to H = 40 mm where the peak soot volume fraction is observed at a radial location of 2.5 mm from the centerline, while soot is observable at the centerline at a height of 30 mm in Fig. 3 (a). Subsequent development involves a net destruction of soot particles through soot oxidation with soot volume fraction in the annular region diminishing more rapidly than in the central region.

Figures 3 (a)-(c) show an excellent agreement between the LII and laser extinction/scattering data for the soot volume fraction with data being within 5-10% of one another at most of the heights where measurements have been obtained. However, there is a tendency for the LII data to underestimate the soot volume fraction on one side of the flame, resulting in slightly asymmetric soot volume fraction profiles in Fig. 3 (b). This effect is more pronounced at the height of 40 mm than elsewhere and is attributable largely to the fact that the LII signal from the far soot peak traverses the flame in order to arrive at the signal detection site and, thus, is subject to increased path length and correspondingly increased absorption of the signal by the soot and PAH species in the flame. This effect may be correctable by estimating and integrating the local extinction of the signal across the flame. Figure 4 similarly shows the integrated soot volume fraction as a function of height. The comparison between the LII and laser extinction/scattering data [8,9] yields reasonably good agreement with the maximum discrepancy being approximately 10% at a height of 30 mm.

The effect of laser fluence on the LII signal is shown in Fig. 5. The laser fluence has been varied from 2.5×10^7 to 4.2×10^8 W/cm^2 using the combination of the half-wave plate and beam splitter, as described earlier. For a laser fluence from 2.5×10^7 to 1.2×10^8 W/cm^2, it can be seen in Fig. 5 that the LII signal increases rapidly as the laser fluence increases. This effect is due to the fact that the soot particle temperature increases as a function of the laser fluence which causes a corresponding increase in the LII signal. In contrast, the LII signal for laser fluence beyond ca. 1.2×10^8 W/cm^2 exhibits a small increase with respect to an increase in laser fluence. The influx of laser energy on the soot particles can cause vaporization of small carbon fragments, such as C_2 and C_3, from the soot particle surface. For sufficiently large laser fluence this vaporization mechanism and corresponding mass loss can become the dominant effect which limits the increase in soot particle temperature and, thus, causes a leveling of the LII signal as shown in Fig. 5. However, the LII signal intensity in this "saturation" regime increases as a weak function of the laser fluence in Fig. 5 similar to the results of Eckbreth [7] in which soot surface temperatures as high as 5000 K were

observed with increasing laser fluence. From the data shown in Fig. 5, it is estimated that the "saturation" regime for the LII signal occurs for laser fluences above 1.2 x 10^8 W/cm^2 in the present studies. During the actual measurements of soot volume fraction. large laser fluence levels in the "saturation" regime, as was used in the present study, have the advantage of being least affected by the effects of the laser beam attenuation across the flame, since the LII signal is a weak function of the laser fluence in this regime. For the results reported here, the LII response varied by less than 5% for the range of laser fluence attenuations (~30% maximum attenuation) encountered in the present study. The observed response of the LII signal to the laser fluence is sensitive to the laser beam intensity profile, the specific focusing arrangement employed for the incident beam and the timing of the boxcar gate pulse with respect to the laser pulse. Other researchers have observed more significant effects of the laser fluence on the LII signal [12] and further research is needed in this area. However, for the conditions described in the present work, reproducible results were always obtained as long as care was taken in the alignment of the optics and achievement of a near-gaussian beam intensity profile.

The spectral response of the LII signal is shown in Fig. 6, where the LII signal is plotted as a function of the detection wavelength. The spectral scan of the LII signal has been obtained by rotating the grating in the monochromator so that the detection wavelength is varied in 10 nm increments. Measurements have been taken at the radial location where the peak soot volume fraction occurs at the 40 mm height for a probe laser beam at the 1064 nm wavelength with a beam diameter of 0.5 mm and an energy of 1.5 mJ/pulse or laser fluence of 9.5 x 10^7 W/cm^2. For the 1064 nm wavelength laser probe beam, interference from light-scattering and PAH fluorescence is minimal in the visible wavelength range, although a fortuitous peak at 532 nm is seen due to the leakage of the 532 nm beam from the laser and corresponding light-scattering at this wavelength. It can be observed that as expected the LII signal exhibits a continuous spectra in the visible wavelength range with the signals decreasing to small levels below 300 nm. The LII spectrum also shows no distinct peaks and

continues up to 750 nm at a nearly constant level. Comparison with computed blackbody radiation curves, as shown in Fig. 6, indicates that the LII spectrum in the 300-450 nm range corresponds to a soot temperature between 5000 and 6000 K, which is higher than the estimated soot vaporization temperature of ca. 4000 K. That the LII spectrum continues at a nearly constant level up to 750 nm and beyond, while the computed radiation curves begin to decline, is attributed to the fact that a large soot number density, and corresponding multiplicity of soot particle size, is present in the probe volume with different soot surface temperatures induced by the laser fluence. Hence, a more continuous and level spectral response is expected as shown in Fig. 6 for a group of soot particles in comparison to a radiation curve computed for a single soot particle surface temperature. From Fig. 6, it can also be observed that by using 1064 nm wavelength probe laser, LII measurements can be taken at nearly any wavelength in the visible range, except near 532 nm for our optical arrangement, due to the absence of interference from PAH fluorescence and light-scattering as noted above, and measurements taken at detection wavelengths of 400 and 700 nm have yielded identical soot volume fraction results.

The heating of the soot particles to such high temperatures may lead one to be concerned about altering the properties of the soot particles. In the present experiments we assume that the soot properties are not seriously affected the large laser fluence before the LII measurements are made. Furthermore, since the LII signals are calibrated against independently measured soot volume fraction values, any changes introduced as long as they are the same throughout the soot field, are compensated for in the calibration procedure. These assumptions will need to be verified in future studies, but are not anticipated to introduce errors any more significant than the present knowledge of soot properties necessarily include.

Figure 7 (a) shows the soot volume fraction measured by LII and the vertically-polarized component of the light-scattering signal (Q_w), while Fig. 7 (b) contains the data for the mean soot particle diameter and the soot number density obtained from these measurements. To obtain the

results shown in Fig. 7 (b), the Q_w and soot volume fraction measurements were analyzed in a manner similar to that described by Santoro et al. [8]. The vertically-polarized light-scattering signal has been obtained for the 532 nm wavelength laser probe beam, and the calibration for the absolute value of Q_w has been obtained by matching with the known value of this signal at a single radial position using measurements by Santoro et al. [8] similar to the calibration procedure for the soot volume fraction. From the soot volume fraction and light-scattering data, which is proportional to the 6th moment of the soot particle diameter distribution, the mean soot particle diameter (D_{63}) and the soot number density (N) can be obtained as follows [8]:

$$D_{63} = \lambda^{4/3} \left(\frac{2Q_{vv}}{3\pi^3 F(\tilde{m}) f_v} \right)^{1/3}, \text{ where} \tag{1}$$

$$F(\tilde{m}) = \left| \frac{\tilde{m}^2 - 1}{\tilde{m}^2 + 2} \right|^2. \tag{2}$$

$$N = \frac{12 f_v}{\pi D_{63}^3} \tag{3}$$

Here, f_v denotes the soot volume fraction while the complex index of refraction, $\tilde{m}$, is taken as (1.57 - 0.56 i) following Dalzell and Sarofim [13]. Similar to light scattering/extinction, the LII/light scattering technique yields the ratio of the sixth to third moment (D_{63}) of the particle diameter. The resultant mean soot particle diameter and the soot number density are again compared with the previous data obtained for this flame using the laser scattering/extinction method [8]. Figure 7(b) shows that the mean soot particle diameters are in very good agreement with the discrepancy being mostly limited to the central region where due to the relatively low signal levels there is the largest uncertainty in both the LII and light-scattering data. The mean soot particle diameter from LII data in the present study ranges from 75-130 nm, while diameters of 60 to 135 nm have been observed by

Santoro et al. [8].

It should be noted that the particle diameters reported, in some cases, exceed the size normally considered to be appropriate for a Rayleigh theory analysis. In fact, the soot particles in this flame are aggregates composed of primary particles which do satisfy the Rayleigh theory limit [14]. Thus, strictly, D and N refer to the volume equivalent diameter and number density, respectively, of these aggregates. Particle morphology effects are not included explicitly in the current study, which would require multiple-angle light scattering measurements. However, such measurements are feasible, in principle, and represent another area where the LII technique can contribute to research related to soot particle property determination.

The soot number density profiles are similarly in reasonably good agreement with the discrepancy again occurring near the centerline. Since the number density is inversely proportional to the cube of the mean soot particle diameter, the factor of two difference in the soot number density near the centerline is caused by the corresponding difference in the mean soot particle diameter shown in Fig. 7(b). Thus, Fig. 7(b) shows that with a single-point or two-dimensional measurements of LII and light-scattering, which can be set up with relative ease, a complete characterization of soot particle properties may be directly obtained.

CONCLUSIONS

From the discussion above, following conclusions concerning the laser-induced incandescence diagnostic of soot volume fraction are made:

(1) Laser-induced incandescence has been used to obtain spatially-resolved measurements of soot volume fraction in laminar diffusion flames, in which comparisons with laser scattering/extinction data yield excellent agreement for both radial profiles and integrated volume fraction. Thus, laser-induced incandescence can be used as an instantaneous, spatially-resolved diagnostic of soot volume fraction without the need for the conventional line-of-sight laser extinction method.

(2) The temporal characteristics of the laser-induced incandescence signal is observed to involve a

rapid rise in intensity followed by a relatively long (ca. 600 ns) decay period subsequent to the laser pulse, while the effect of laser fluence is manifest in non-linear and saturated response of the laser-induced incandescence signal with the transition occurring at a laser fluence of approximately 1.2 x 10^8 W/cm^2 for laser pulse of ca. 7 ns in duration.

(3) Spectral response of the laser-induced incandescence involves a continuous spectrum in the visible wavelength range due to the blackbody nature of the emission, where the spectral response for 300-450 nm wavelength range indicates a soot surface temperature of ca. 5000 K with the spectrum continuing at a nearly level intensity up to 750 nm wavelength due to the multiplicity of the soot particle sizes in the probe volume.

(4) Simultaneous measurements of LII and the vertically-polarized light-scattering yield encouraging results concerning the mean soot particle diameter and number concentration; thus significant applications exist in two-dimensional imaging and simultaneous measurements of laser-induced incandescence and light-scattering to generate a complete soot property characterization.

ACKNOWLEDGEMENTS

This material is based upon work supported by the Air Force Office of Scientific Research under Award No. F49620-92-J-0314 with Dr. Julian Tishkoff as contract manager and their support is gratefully acknowledged. The authors would also like to thank J. A. Pinson and S. Gupta of Penn State for many useful discussions and J. E. Harrington, C. R. Shaddix and K. C. Smyth of the National Institute of Standards and Technology for providing us with their results on the effects of laser fluence on LII signals. We would also like to acknowledge the reviewers for their suggestions regarding the light scattering analysis and the effects of aggregates on the interpretation of the results of this work.

REFERENCES

1. Melton, L. A. *Appl. Opt.* 23:2201-2208 (1984).

2. Dasch, C. J. *Appl. Opt.* 23:2209-2215 (1984).

3. Eckbreth, A. C., Bonczyk, P. A. and Verdieck, J. F. *Prog. Energy Combust. Sci.* 5:253-322 (1979).

4. Tait, N. P. and Greenhalgh, D. A. *Proceedings of the "Optical Methods and Data Processing In Heat Transfer and Fluid Flow" Conference*. London, April 1992.

5. Dec, J. E., zur Loye, A. O. and Siebers, D. L. *SAE Technical Papers Series* SAE-910224. Society of Automotive Engineers, PA 1991.

6. Dec J. *SAE Technical Papers Series* SAE-920115. Society of Automotive Engineers, PA 1992.

7. Eckbreth, A. C. *J. Appl. Physics* 48:4473-4479 (1977).

8. Santoro, R. J., Semerjian, H. G. and Dobbins, R. A. *Combust. Flame* 51:203-218 (1983).

9 Santoro, R. J., Yeh, T. T., Horvath, J. J., and Semerjian, H. G. *Combust. Sci. and Tech.* 53:89-115 (1987).

10. Puri, R., Moser, M., Santoro, R. J. and Smyth, K. C. *Twenty-Fourth Symposium (International) on Combustion*. The Combustion Institute, Pittsburgh, 1992, pp. 1015-1022.

11. Miller, J. H., Mallard, W. G. and Smyth, K. C. *Combust. Flame* 47:205-214 (1982).

12. Shaddix, C.R., Harrington, J.E. and Smyth, K.C., personal communication

13. Dalzell, W. H. and Sarofim, A. F. *Trans. ASME J. Heat Transfer* 91:100-104 (1969).

14. Puri, R., Richardson, T. F., Santoro, R. J. and Dobbins, R. A. *Combust. Flame* 92:320-333 (1993).

Figure Captions

Fig. 1 Optical arrangement for laser-induced incandescence measurements.

Fig. 2 Temporal response of the laser-induced incandescence.

Fig. 3 Radial profiles of the soot volume fraction obtained via laser-induced incandescence and laser scattering/extinction at several heights (H) above fuel tube exit of the burner (a) H = 10, 20, and 30 mm; (b) H = 40 and 50 mm; and (c) H = 60 and 70 mm.

Fig. 4 Integrated soot volume fraction plotted as a function of height above the fuel tube exit of the burner.

Fig. 5 Effect of laser fluence on the laser-induced incandescence signal.

Fig. 6 Spectral response of the laser-induced incandescence where incident laser light at a wavelength of 1064 nm was used to obtained the spectrum shown.

Fig. 7(a) Radial profiles of the soot volume fraction and vertically-polarized light-scattering signal, Q_{vv}, at a height, H, of 40 mm above the fuel tube exit of the burner.

Fig. 7(b) Radial profiles of the mean soot particle diameter, D_{63}, and soot number concentration, N, at a height, H, of 40 mm above the fuel tube exit of the burner.

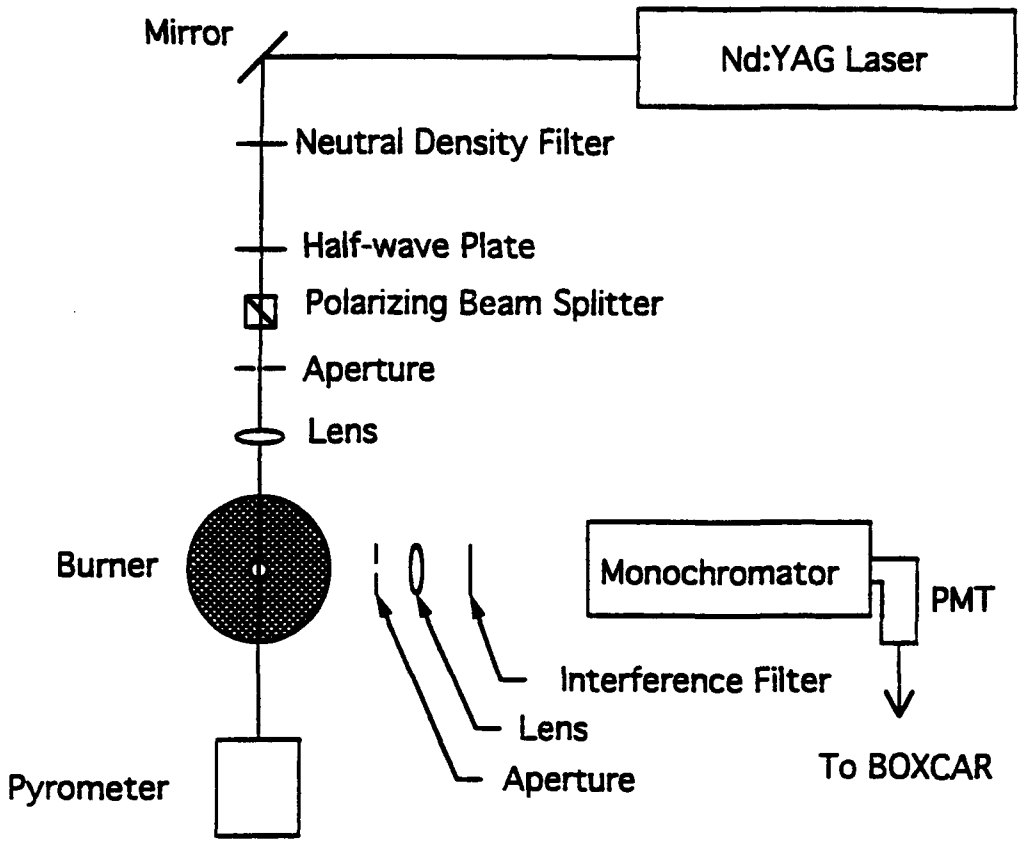
Mirror
Nd:YAG Laser
Neutral Density Filter
Half-wave Plate
Polarizing Beam Splitter
Aperture
Lens
Burner
Monochromator
PMT
Interference Filter
Lens
Aperture
To BOXCAR
Pyrometer

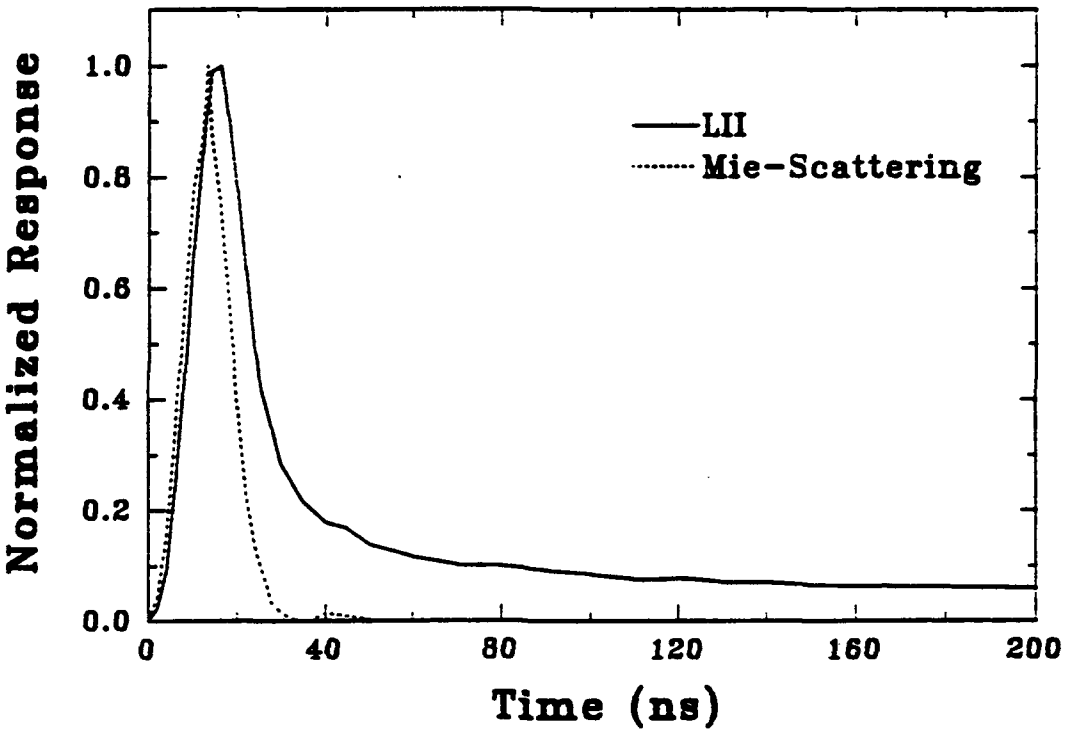
Normalized Response
1.0
0.8
0.6
0.4
0.2
0.0
0
40
80
120
160
200
Time (ns)
LII
Mie-Scattering

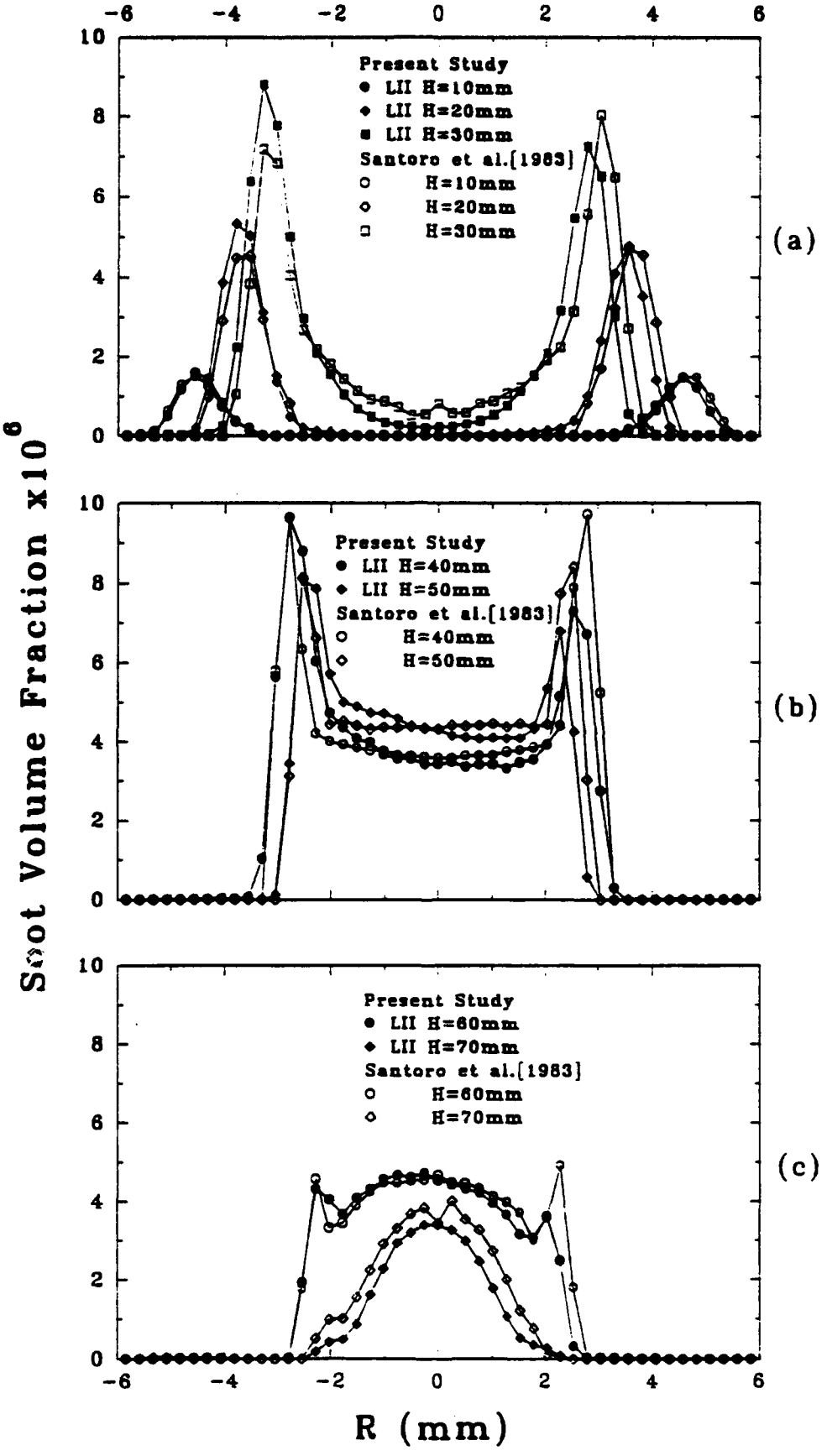
Present Study
LII H=10mm
LII H=20mm
LII H=30mm
Santoro et al.[1983]
H=10mm
H=20mm
H=30mm
(a)
Present Study
LII H=40mm
LII H=50mm
Santoro et al.[1983]
H=40mm
H=50mm
(b)
Present Study
LII H=60mm
LII H=70mm
Santoro et al.[1983]
H=60mm
H=70mm
(c)
Soot Volume Fraction x10^6
R (mm)

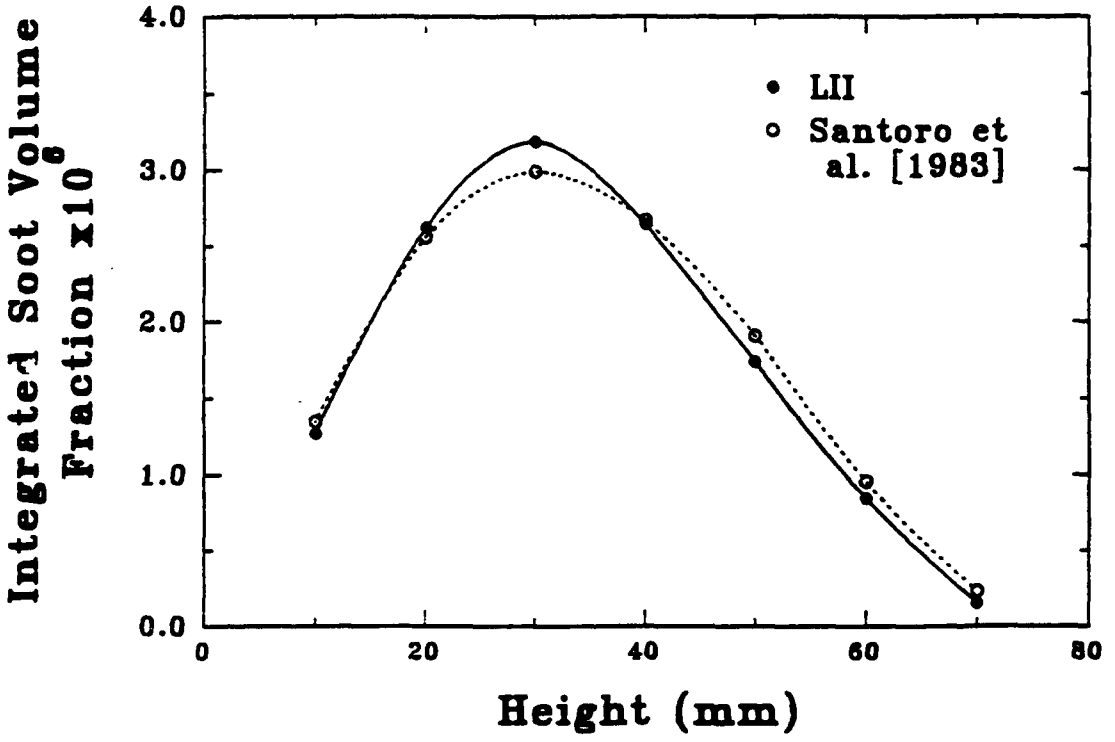
Integrated Soot Volume Fraction x10^6
4.0
3.0
2.0
1.0
0.0
0
20
40
60
80
Height (mm)
• LII
○ Santoro et al. [1983]

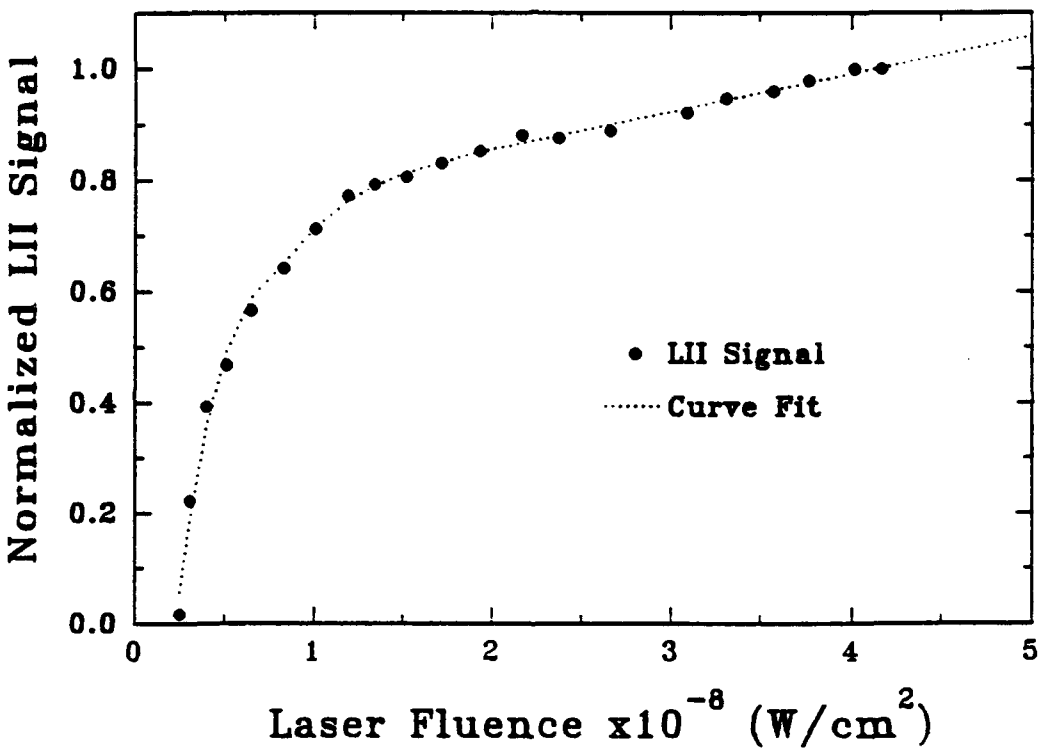
Normalized LII Signal
1.0
0.8
0.6
0.4
0.2
0.0
0
1
2
3
4
5
LII Signal
Curve Fit
Laser Fluence x10^{-8} (W/cm^2)

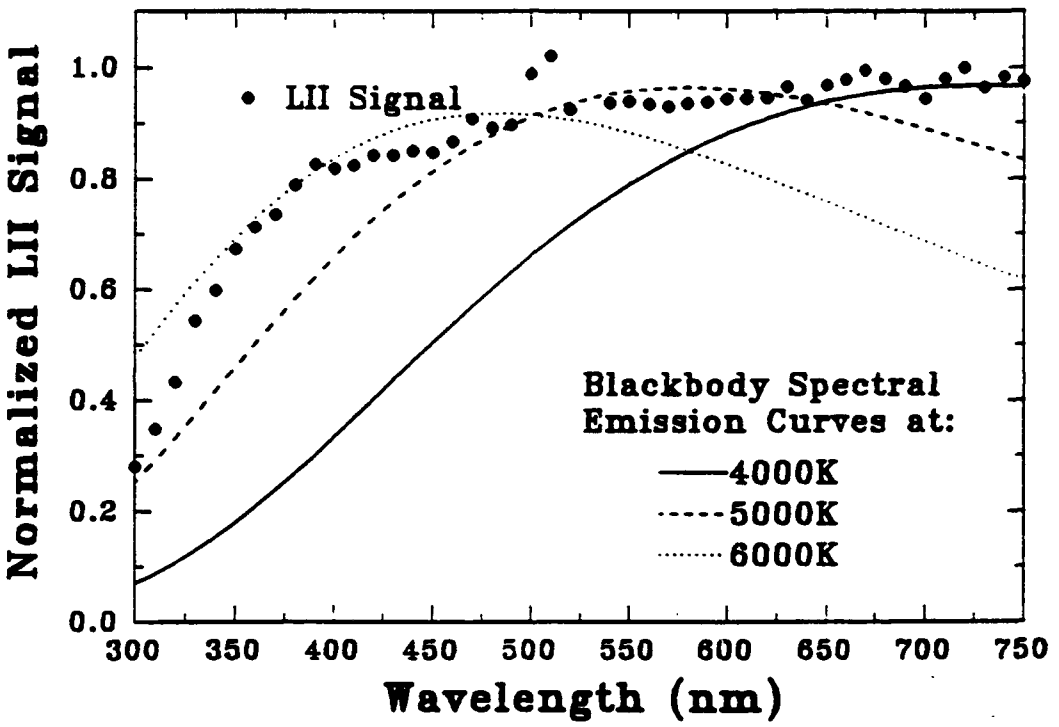
Normalized LII Signal
1.0
0.8
0.6
0.4
0.2
0.0
LII Signal
Blackbody Spectral
Emission Curves at:
4000K
5000K
6000K
300
350
400
450
500
550
600
650
700
750
Wavelength (nm)

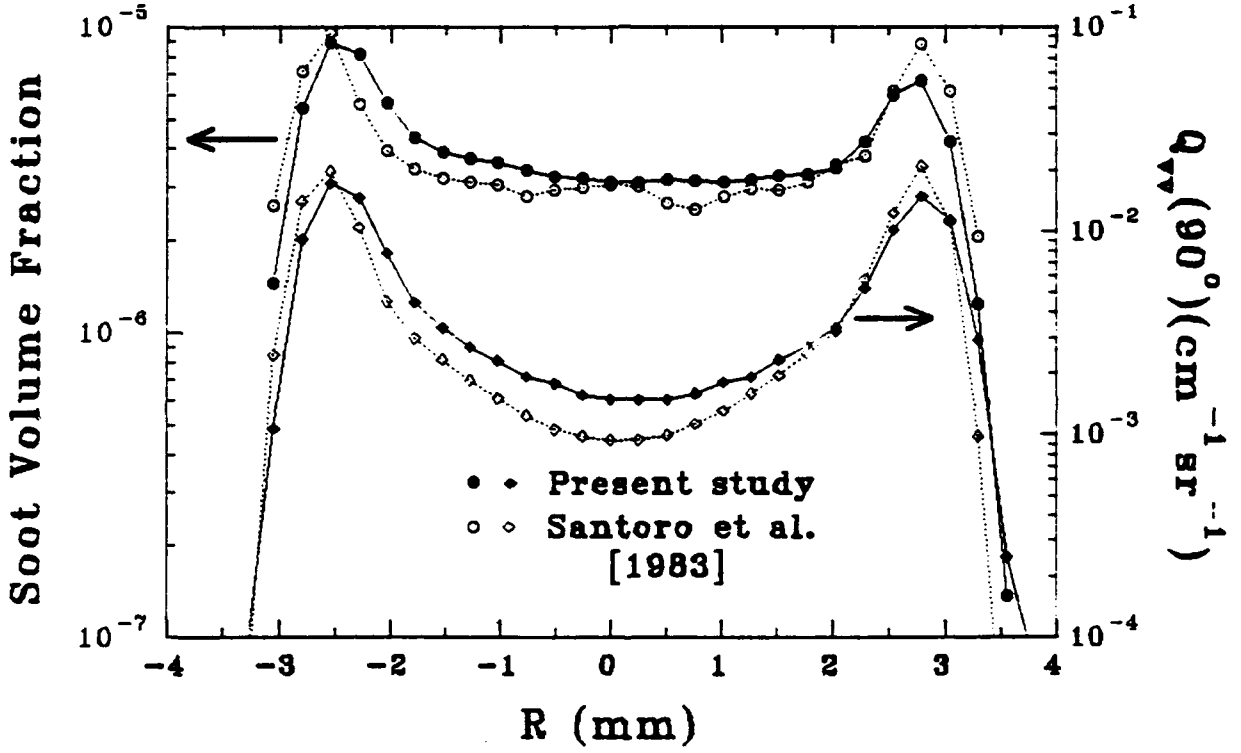
Soot Volume Fraction
10^{-5}
10^{-6}
10^{-7}
10^{-1}
10^{-2}
10^{-3}
10^{-4}
$q_{vv}(90^o)(cm^{-1}\,sr^{-1})$
−4
−3
−2
−1
0
1
2
3
4
R (mm)
Present study
Santoro et al. [1983]

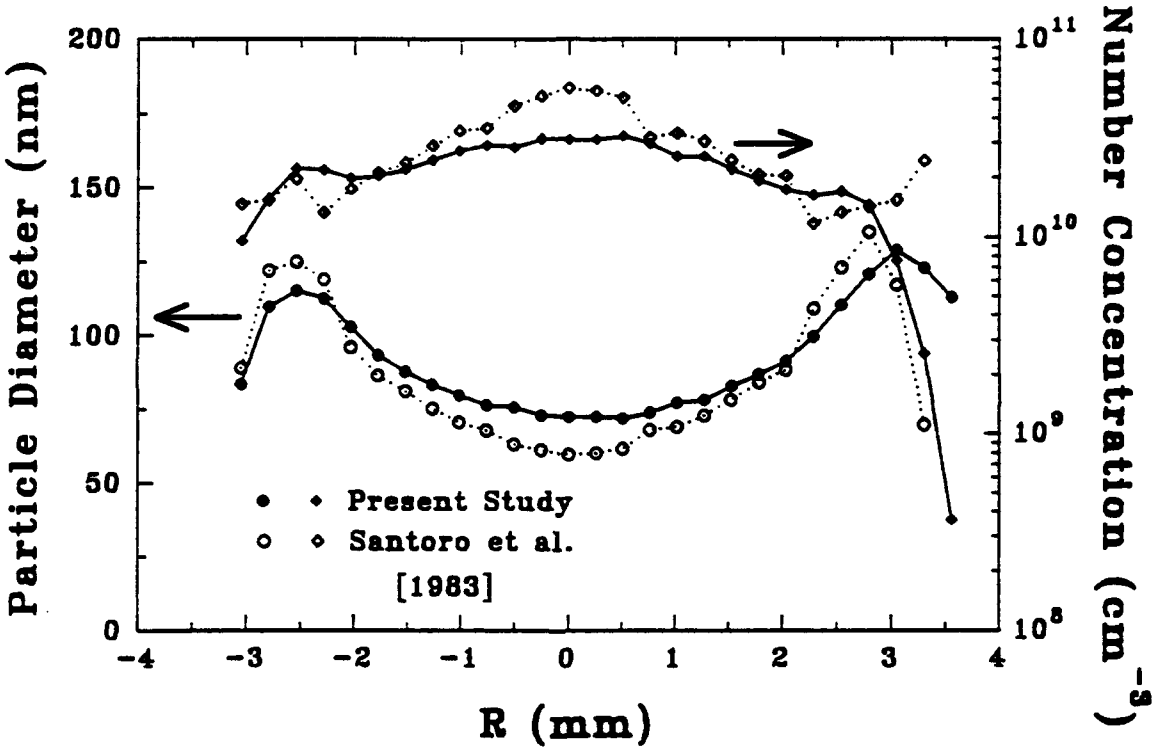
Particle Diameter (nm)
Number Concentration (cm^{-3})
R (mm)
Present Study
Santoro et al.
[1983]
200
150
100
50
0
10^{11}
10^{10}
10^{9}
10^{8}
−4
−3
−2
−1
0
1
2
3
4

Approved for public release;
distribution unlimited.

A[illegible] FORCE OF SCIENTIFIC RESEARCH (AFSC)
[illegible]TICE OF TRANSMITTAL TO DTIC
[illegible]s technical report has been reviewed and is
[illegible]roved for public release IAW AFR 190-12
[illegible]tribution is unlimited.
[illegible]an Boggs
[illegible]TINFO Program Manager